22

PET Imaging in Pediatric Disorders

Hossein Jadvar, Leonard P. Connolly, Frederic H. Fahey, and Barry L. Shulkin

Development and validation of applications for positron emission tomography (PET) in pediatrics has proceeded more slowly than in adult medicine, partly because diseases to which PET has been most widely applied in adults are uncommon in pediatrics. Only about 2% of all cancers, for example, occur before 15 years of age. Experience has therefore been gained more slowly in pediatrics. Accrual of experience has been further slowed because there are few PET units in pediatric hospitals. The labor-intensive nature of imaging sick children has limited the ability of adult-oriented PET centers, which are faced with a shortage of available imaging slots, to take on a substantial number of time-consuming, challenging pediatric cases. Despite these considerations, PET, and more recently the hybrid positron emission tomography-computed tomography (PET/CT) imaging systems, are emerging as important tools in pediatric nuclear medicine. In this chapter, we review the clinical applications of PET in pediatrics with an emphasis on the more-common applications in epilepsy and oncology. General considerations in patient preparation and radiation dosimetry are also discussed.

Patient Preparation

Preparation of children and parents for nuclear medicine imaging has been thoroughly reviewed elsewhere (1, 2). As with any imaging study, gaining the trust and allaying the fears of both the patient and the parents are essential before attempting to image. Because parental attitudes and anxieties are readily conveyed to children, it is essential that the parents be well informed and cooperative if their child's trust is to be gained. Patient cooperation, once achieved, may be assisted by relatively simple methods. Sheets wrapped around the body, sandbags, and/or special holding devices are often sufficient for immobilization. Parents may accompany their child during the course of a study to provide emotional support. However, on occasion, an anxious parent may actually impair the performance of the study.

Sedation is indicated when, on the basis of careful consideration, it is anticipated that simpler approaches will be inadequate. Sedation protocols, particularly regarding the recommended medications and the level of sedation required for an imaging procedure, vary from institution to institution. Guidelines such as those advanced by the Society of Nuclear Medicine (3) are useful in developing an institutional sedation program and a sedation formulary.

Also important to consider is the potential effect of sedatives on ^{18}F-2-deoxy-D-glucose (FDG) distribution. Many sedatives may affect cerebral metabolism. When performing FDG-PET of the brain, it is best if sedatives are not administered for 30 min after FDG administration because it is during this interval that the majority of cerebral FDG uptake occurs. Sedatives are not known to cause significant changes in tumoral metabolism and can be administered at any time relative to FDG administration for studies of tumors outside the central nervous system (4). During this time, the patient should be kept quiet and inactive to reduce regional stimulation of the cerebral cortex, which might confuse interpretation of the results.

Other important technical issues specific to performing PET studies in pediatric patients (e.g. consent, intravenous access, bladder catheterization) have recently been reviewed (5, 6). The recent introduction of PET/CT imaging systems also present unique issues that will need to be addressed. Kaste et al. (7) has reviewed the experience with implementing PET/CT at a tertiary pediatric hospital. Issues such as physical location of the PET/CT unit, the roles of CT and nuclear medicine technologists, and the methodology for study interpretation are discussed. Additional important considerations deliberated are the use of intravenous and sugar-free oral contrasts for the CT portion of the PET/CT examinations and the management of hyperglycemia.

Table 22.1. Radiation dosimetry for ^{18}F-2-deoxy-D-glucose (FDG).

	1 year	5 years	10 years	15 years	Adult
Mass (kg)	9.8	19.0	32.0	55.0	70.0
Administered activity (MBq)	54.5	105.6	177.8	305.6	389.0
Bladder	32.1	33.8	49.8	64.2	62.2
Brain	2.6	3.6	5.3	8.6	10.9
Heart	19.1	21.1	21.3	24.8	24.1
Kidneys	5.2	5.7	6.4	7.6	8.2
Red marrow	3.3	3.4	3.9	4.3	4.3
Effective dose (mSv)	5.2	5.3	6.4	7.6	7.4

The doses are reported in mSv (8). Patient masses represent the 50% percentile for that age (9).

Radiation Dosimetry

Several factors affect the dosimetry of positron emitters relative to single photon imaging agents. On the one hand, the energy per photon is higher (511 keV as compared to 140 keV for ^{99m}Tc), and there are two photons emitted per disintegration, which leads to much higher energy per unit activity than with most single photon agents. However, the higher photon energy also leads to a smaller fraction of the photons being absorbed within the patient. Table 22.1 summarizes the dosimetry of FDG for selected organs as well as the effective dose in the pediatric population based upon the administered activity of 5.55 kBq/kg (0.15 “Ci/kg).

Because the administered activities are scaled by body weight, the doses are similar across the age range, being slightly higher in adults. The effective dose is 5.2 and 7.4 mSv for the 1-year-old child and the adult, respectively. The critical organ is the bladder wall, with the dose being six to eight times higher than the effective dose. Table 22.2 compares the effective dose from FDG to a number of commonly used single photon imaging agents.

Table 22.2 illustrates that the radiation-absorbed dose to the patient from an FDG-PET study is very similar to the dose received from other nuclear medicine imaging procedures (4, 10, 11).

In pediatric imaging, the parents of the patient often prefer to remain with the patient during the procedure. The exposure rate constants for ^{18}F and ^{99m}Tc are 0.0154 and 0.00195 mR/h per MBq at 1 m, respectively. The difference is primarily due to the higher photon energy for ^{18}F as compared to ^{99m}Tc and the fact that two photons are emitted per disintegration. It is therefore prudent to consider the radiation exposure to the parent during these procedures. As shown in Table 22.1, pediatric patients receive a range of administered activities depending on patient size. The following assumptions are made: the patient receives 260 MBq and is considered to be a point source with no self-absorption. The patient sits in a preparatory room for 60 min during uptake and then is imaged for 60 min. These assumptions are considered quite conservative; that is, these will probably lead to an overestimation of the radiation dose to the parent. Table 22.3 estimates the total exposure to the parent during both the uptake and imaging periods, provided the parent maintains the specified distance from the patient.

Even if the parent stayed within 1 m of the patient during the entire uptake and imaging periods, the exposure to the parent would be no more than 5.5 mR. Therefore, the parents can be allowed to stay with the patient during the procedure but are instructed to stay as far from the patient as they feel comfortable.

Hybrid PET/CT scanners use the CT portion of the examination for attenuation correction. The dose to the patient from CT can vary greatly, depending on the tube voltage and current and the size of the patient. Table 22.4 summarizes the radiation dose to patients from the CT transmission as a function of tube voltage (based on a phantom study using phantoms of various sizes).

Table 22.2. Effective dose in pediatric patients for a variety of radiopharmaceuticals.

Radiopharmaceutical	Maximum administered activity (MBq)	1 year	5 years	10 years	15 years	Adult
FDG	389	5.2	5.3	6.4	7.6	7.4
^{67}Ga-Citrate	222	19.9	19.9	20.3	22.7	22.2
^{99m}Tc HMPAO	740	5.1	5.4	5.8	6.4	6.9
^{99m}Tc MDP	740	2.8	2.8	3.7	4.1	4.2
^{99m}Tc SestaMIBI	740	4.7	4.6	5.4	5.8	5.8

The doses are reported in mSv. The maximum administered activity is that which would be administered to a 70-kg adult. The pediatric dose administered is scaled by the patient’s weight as in Table 22.1 (8, 9). Patient masses represent the 50% percentile for that age (9).

Table 22.3. Total exposure to the parent from a patient receiving 260 MBq of ^{18}F for a positron emission tomography (PET) study.

Distance from patient during uptake period (m)	Distance from patient during imaging period (m)	Total exposure to parent (mR)
1	1	5.5
1	2	4.0
2	2	1.4
2	3	1.1

It is assumed that the parent stayed with the patient during a 60-min uptake period and a 60-min imaging period.

Table 22.4. Radiation dose from computed tomography (CT) transmission as a function of tube voltage.

Kvp	Newborn	1 year	5 years	10 years	Medium adult
80	7.0	5.7	4.5	3.8	1.5
100	13.5	11.3	9.0	7.9	3.5
120	21.4	18.2	14.9	12.9	6.0
140	30.1	25.8	21.8	18.9	9.0

All doses are reported in mGy. All data were obtained at 130 mA and a pitch of helical 1.5:1 (12).

Smaller patients receive a substantially higher dose than adults from the same CT acquisition parameters. For example, the radiation dose to a 10-year-old is approximately twice that to a medium-sized adult for the same CT acquisition parameters. An alternative to using CT for attenuation correction is to use rotating rod sources. With a total activity in the rods of 370 MBq, the dose to the patient is between 0.05 and 0.2 mGy for a 15-min acquisition, based on a phantom study using phantoms of different sizes (12). Thus, the dose to the patient from a CT scan used for attenuation correction is substantially higher than that associated with the rotating rods sources. However, the CT scan provides anatomic correlation to the functional images, a feature that is not available using the rod sources.

Comparing the values in Tables 22.1 and 22.4, the dose to the patient from the CT portion of the scan can be equal to, if not higher than, the dose received from the radiopharmaceutical. Thus, the acquisition parameters for the CT portion of the scan should be tailored to the patient's size. For diagnostic CT, reduction of exposure by 30% to 50% relative to an adult has been suggested (13). Reducing the milliamps (mA) proportionately decreases the absorbed radiation dose without significant loss in the information provided. In addition, there is the potential to further reduce the tube voltage and current without adversely affecting the quality of the attenuation correction in those cases where anatomic correlation is not required.

PET in Pediatric Neurology

Normal Brain Development

An understanding of the normal brain development and evolution of cerebral glucose utilization is important when FDG-PET is considered as a diagnostic functional imaging study. Functional maturation proceeds phylogenetically. Glucose metabolism is initially high in the sensorimotor cortex, thalamus, brainstem, and cerebellar vermis. During the first 3 months of life, glucose metabolism gradually increases in the basal ganglia and in the parietal, temporal, calcarine, and cerebellar cortices. Maturation of the frontal cortex, which proceeds from lateral to medial, and of the dorsolateral cortex occur during the second 6 months of life. Cerebral FDG distribution in children after the age of 1 year resembles that of adults (Figure 22.1).

Childhood Epilepsy

Epilepsy is a relatively common and potentially devastating neurologic condition during childhood. Its incidence in children and adolescents is between 40 and 100 per 100,000 (17). The 1990 National Institutes of Health Consensus Conference on Surgery for Epilepsy estimated that 10% to 20% of epilepsy cases prove medically intractable and that 2,000 to 5,000 epilepsy patients per year can benefit from surgical resection of the seizure focus (18).

Accurate preoperative localization of the epileptogenic region is an essential but difficult task that is best accomplished by finding a concordance between results obtained with clinical examination, electroencephalography (EEG), neuropsychologic evaluation, and imaging studies. Computed tomography (CT) and magnetic resonance imaging (MRI) are used to detect anatomic lesions that may cause the seizures. However, structural lesions occur in a relatively small percentage of patients with epilepsy and, when such lesions are detected, they may not necessarily correspond to the epileptogenic region (19). Ictal or interictal single photon emission tomography (SPECT) evaluation of regional cerebral blood flow (rCBF) with tracers such as ^{99m}Tc-hexamethylpropylene (^{99m}Tc-HMPAO) and ^{99m}Tc-ethyl cysteinate dimer (^{99m}Tc-ECD) can localize the epileptogenic region in the presence or absence of structural abnormalities. The characteristic appearance of an epileptogenic region is relative zonal hyperperfusion on ictal SPECT and relative zonal hypoperfusion on interictal SPECT. The sensitivity of ictal rCBF tracer SPECT may approach 90% whereas that of interictal SPECT is in the range of 50% (20). The utility of ictal SPECT is somewhat reduced by the difficulty in coordinating tracer administration with seizures. Noninvasive evaluation is often unsuccessful in precisely localizing an epileptogenic region. As a result, surgical placement of

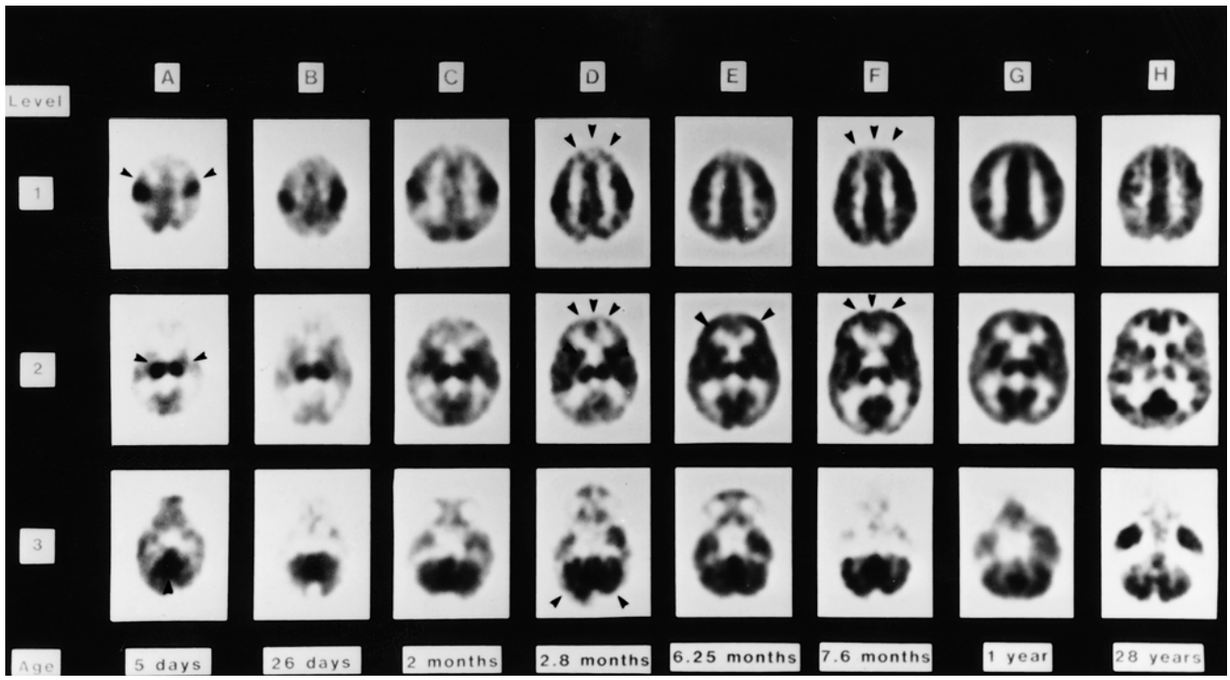

Figure 22.1. Normal brain maturation. Positron emission tomography (PET) scans show ontogenic changes in local cerebral glucose metabolism of the normal human infant. (**a**) In the 5-day-old infant, glucose metabolism is highest in the sensorimotor cortex, thalamus, cerebellar vermis (*arrows*), and brainstem (not shown). (**b**–**d**) Glucose metabolism increases gradually in the parietal, temporal, and calcarine cortices, basal ganglia, and cerebellar cortex (*arrows*), especially during the second and third months. (**e**) In the frontal cortex, glucose metabolism increases first in the lateral prefrontal regions by approximately 6 months. (**f**) By about 8 months, glucose metabolism also increases in the medial aspects of the frontal cortex (*arrows*) as well as the dorsolateral occipital cortex. (**g**) By 1 year of age, the glucose metabolic pattern resembles that of a normal adult, although the metabolic rates are two- to threefold elevated in comparison to values expected in normal adults. (Photo kindly provided by Harry Chugani, MD. From Chugani HT. Positron emission tomography. In: Berg BO, editor. Principles of Child Neurology. New York: McGraw-Hill, 1996:113–128.)

electrode grids on the brain surface or insertion of depth electrodes becomes necessary.

FDG-PET has proven useful in preoperative localization of the epileptogenic region (Figure 22.2) (21). FDG-PET is generally performed following an interictal injection. Although metabolic alterations might be localized better ictally than interictally, the relatively short half-life of ^{18}F limits the window of opportunity during which it can be administered ictally. Even when FDG can be administered at seizure onset, the approximately 30-min brain uptake time of FDG means that the study may depict periictal as well as ictal FDG distribution. Ictal FDG studies may also show areas of seizure propagation that could be confused with the actual seizure focus. Despite these considerations, some favorable results have been reported employing ictal PET for patients with continuous or frequent seizures (22).

For interictal PET, FDG should be administered in a setting such as a quiet room with dim lights where environmental stimuli are minimal during the 30 min following FDG administration. It is best to have the child remain awake with minimal parental interaction during this period. EEG monitoring is essential to identify seizure ac-

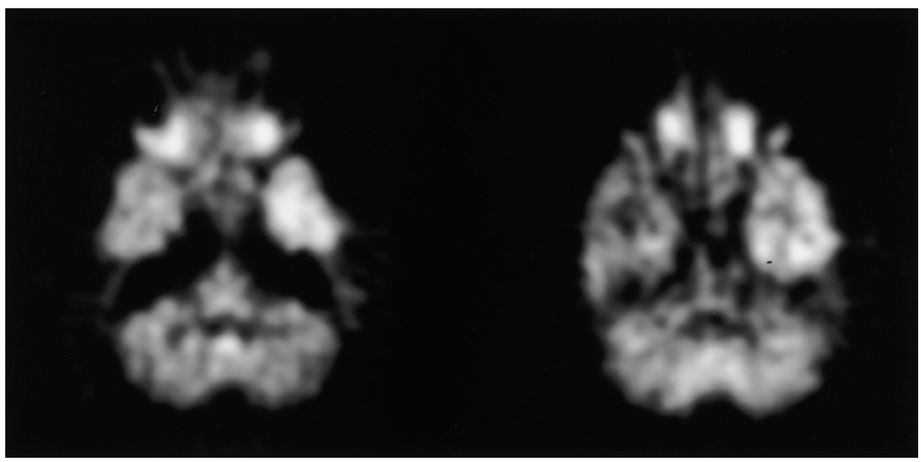

Figure 22.2. Transverse brain FDG-PET scan of a 14-year-old girl shows a hypometabolic epileptogenic right temporal lobe. (Reprinted with permission from Jadvar H, Connolly LP, Shulkin BL, Treves ST, Fischman AJ. Positron-emission tomography in pediatrics. Nuclear Medicine Annual 2000;53–83.)

tivity that might affect FDG distribution. The sensitivity of interictal FDG-PET approaches that of ictal rCBF SPECT in localizing the epileptogenic region, which is detected as regional hypometabolism. Importantly, the hypometabolism may predominantly affect cortex bordering the epileptogenic focus. Epileptic activity may originate in cortical areas bordering the hypometabolic regions rather than the hypometabolic region itself (23).

Incorporation of FDG-PET into preoperative evaluation of epilepsy patients reduces the need for intracranial EEG monitoring and the cost of preoperative evaluation (24). The best results have been obtained in temporal lobe epilepsy, for which metabolic abnormalities may be evident in as many as 90% of surgical candidates (24, 25). Extratemporal epileptogenic regions are more difficult to identify, but some success has been achieved in children with intractable frontal lobe epilepsy and normal CT or MRI studies (26).

FDG-PET has been reported as being of particular help in the evaluation of infantile spasms, a subtype of seizure disorder. This condition, which has an incidence of 2 to 6 per 10,000 live births, consists of a characteristic pattern of infantile myoclonic seizures and is frequently associated with profound developmental delay despite medical treatment (16, 27). Before the availability of FDG-PET, surgical intervention was attempted and successful in only isolated instances. Incorporation of FDG-PET into the evaluation of children with infantile spasms has resulted in identification of a substantial number of children who benefit from cortical resection. FDG-PET has revealed marked focal cortical glucose hypometabolism associated with malformative or dysplastic lesions that are not evident on anatomic imaging. There is marked decline in seizure frequency and in some patients reversal of developmental delay when a single metabolic abnormality that correlates with EEG findings is shown by FDG-PET. Patients with bitemporal hypometabolism on FDG-PET have a poor prognosis and typically are not candidates for resective surgery (27–31).

In addition to FDG, PET tracers that assess altered abundance or function of receptors, enzymes, and neurotransmitters in epileptogenic regions have been applied to localizing the epileptogenic region. Among alterations that have been observed are relatively reduced uptake of ^{11}C-flumazenil, a central benzodiazepine receptor antagonist, and ^{11}C-labeled (*S*)-(*N*-methyl) ketamine, which binds to the *N*-methyl-D-aspartate receptor-gated ion channel (32–36). Relative increases in uptake of ^{11}C-carfentanil, a selective mu opiate receptor agonist, and ^{11}C-deuterium-deprenyl, an irreversible inhibitor of monoamine oxidase type B (MAO-B) have also been described (37, 38).

Other Neurological Applications

PET with ^{15}O-water has also been investigated in infants with intraventricular hemorrhage and hemorrhagic infarction and in infants with hypoxic–ischemic encephalopathy (39, 40). Cerebral blood flow was markedly reduced not only in the hemorrhagic areas but also in the remainder of the involved hemisphere, suggesting that neurologic deficits may be caused by ischemia rather than the presence of blood within the brain parenchyma or cerebral ventricles (39). In full-term infants with perinatal asphyxia, diminished blood flow to the parasagittal cortical regions suggested that injury to the brain in these infants was also ischemic in etiology (40).

PET has also been employed to study the pathophysiology of many other childhood brain disorders such as autism (41), attention deficit hyperactivity disorder (42), schizophrenia (43), sickle cell encephalopathy (44), anorexia and bulimia nervosa (45, 46), Rasmussen's syndrome (47), Krabbe's disease (48), Sturge–Weber syndrome (49), and cognitive impairment in Duchenne muscular dystrophy (50). However, the exact role of PET in these clinical settings remains unclear. Further experience may result in expanded role of PET in many childhood neurologic disorders.

PET in Pediatric Cardiology

Currently, PET plays a relatively minor role in pediatric cardiology. Quinlivan et al. (51) have reviewed the cardiac applications of PET in children. PET with ^{13}N-ammonia has been employed to measure myocardial perfusion in infants after anatomic repair of congenital heart defects and after Norwood palliation for hypoplastic left heart syndrome (52). Infants with repaired heart disease had higher resting blood flow and less coronary flow reserve than previously reported for adults. Infants with Norwood palliation also had less perfusion and oxygen delivery to the systemic ventricle than the infants with repaired congenital heart lesion, explaining in part the less favorable outcome for patients with Norwood palliation. Evaluation of myocardial perfusion with ^{13}N-ammonia PET in infants following a neonatal arterial switch operation has demonstrated that patients with myocardial perfusion defects may have a more complicated postoperative course (53).

A major application of PET in adult cardiology is the assessment of myocardial viability with FDG as a tracer for glucose metabolism. A recent study evaluated regional glucose metabolism and contractile function by gated FDG-PET in seven infants and seven children after arterial switch operation and suspected myocardial infarction (54). Gated FDG-PET was found to contribute pertinent information to guide additional therapy including high-risk revascularization procedures. Recent reports have also provided evidence for the utility of PET in the assessment of myocardial perfusion and viability in infants and children with coronary abnormalities (55, 56). In another study in children with Kawasaki disease, PET with ^{13}N-ammonia and FDG showed abnormalities in about 60% of patients during the acute and subacute stages and about 40% of patients in the convalescent stage of disease (57). PET was valuable in assessing immunoglobulin therapy response at differing

doses and administration schedules. ^{13}N-ammonia PET may also reveal reduction of coronary flow reserve in children with Kawasaki disease and angiographically normal epicardial coronary arteries (58). Beyond the more common assessment of myocardial perfusion and oxidative metabolism, PET has been used to study such fundamental functional abnormalities as mitochondrial dysfunction in children with hypertrophic or dilated cardiomyopathy (59). Dynamic PET with ^{11}C-acetate demonstrated reduced myocardial Kreb cycle activity (i.e., decreased oxidative metabolism) in children with cardiomyopathy despite normal myocardial perfusion. The diminished oxidative metabolism was associated with compensatory increased glycolytic activity as demonstrated on FDG-PET.

PET in Pediatric Oncology

The incidence of cancer is estimated to be 133.3 per million children in the United States (60). Although cancer is much less common in children than in adults, it is still an important cause of mortality in pediatrics. Approximately 10% of deaths during childhood are attributable to cancer, making it the leading cause of childhood death from disease (61).

Childhood cancers often differ from those encountered in adults, as is illustrated in Table 22.5, which delineates the estimated incidences of the more commonly encountered cancers in American children. Of the adult cancers to which FDG-PET has been most widely applied, only lymphomas and brain tumors occur with an appreciable incidence in children. However, the diagnostic utility of FDG-PET and its impact on patient management have been reported for many pediatric cancers (62–64). In decreasing order of frequency, PET led to important changes in clinical management of lymphoma (32%), brain tumors (15%), and sarcomas (13%) (63).

Before reviewing the applications of PET in pediatric oncology, it is important to consider potential causes of confusion on FDG-PET that relate to physiologic FDG distribution in children. High FDG uptake in thymus (65–67) and in skeletal growth centers, particularly the long bone physes, are two important physiologic variations in FDG distribution encountered in children (Figures 22.3, 22.4). With the introduction of PET/CT imaging systems, it has been recognized that elevated FDG uptake in the normal brown adipose tissue may also be a source of false-positive findings (68, 69). The common anatomic areas involved include the neck and shoulder region, axillae, mediastinum, and the paravertebral and perinephric regions. Neck brown fat hypermetabolism is seen more commonly in the pediatric than in the adult population (15% versus 2%; *P* less than 0.01) and appears to be stimulated by cold temperatures (68, 69). Recent data have shown that brown fat metabolic activity may be suppressed pharmacologically (e.g., propranolol) (70).

Other potential pitfalls, which also apply to imaging adults, include variable FDG uptake in active skeletal muscles, the myocardium, the thyroid gland, and the gastrointestinal tract, as well as accumulation of FDG excreted into the renal pelves and bladder, and possible tracer accumulation in draining lymph nodes from extravasated tracer at the time of injection (71). Diffuse high bone marrow and splenic FDG uptake following adminis-

Table 22.5. Cancer incidence rates per million children younger than 15 years of age in the United States as derived from the Surveillance, Epidemology, and End Results (SEER) and reported in reference.

	Total[a]			Males		Females		Male:Female	Whites		Blacks		White:Black
Histology	No.	Rate	(%)	No.	Rate	No.	Rate		No.	Rate	No.	Rate	
All histologic types	10,555	133.3	100.0	5711	140.9	4844	125.1	1.13	8756	139.5	1064	108.3	1.29
Acute lymohoid leukemia	2484	30.9	23.2	1383	33.7	18.0	1.20	2092	32.9	169	16.9	1.95	
All central nervous system	2205	27.6	1195	29.3	1010	26.0	1.13	1847	29.3	239	23.8	1.23	
Astrocytomas and gliomas	1329	16.8	12.6	692	17.1	637	16.2	1.06	1130	17.9	144	14.3	1.25
Primitive neuroectodermal	532	6.6	5.0	311	7.7	221	5.6	1.38	433	6.8	58	5.9	1.15
Other CNS	344	4.3	3.2	192	4.6	152	3.9	1.18	284	4.6	37	3.6	1.28
Neuroblastoma	74	9.7	7.3	389	9.8	365	9.6	1.02	632	10.2	78	7.8	1.31
Non-Hodgkin's lymphoma	666	8.4	6.3	484	12.0	182	4.6	2.61	578	9.1	53.	5.4	1.69
Wilm's tumor	638	8.1	6.1	287	6.9	351	8.9	0.78	520	8.3	94	9.4	0.88
Hodgkin's disease	511	6.6	5.0	295	7.4	216	5.6	1.32	451	7.3	46	4.7	1.55
Acute mycloid leukemia	454	5.6	4.2	224	5.5	230	6.0	0.92	358	5.8	47	4.8	1.21
Rhabdomyosarcoma	354	4.5	3.4	211	5.2	143	3.6	1.44	294	4.7	40	4.1	1.15
Retinoblastoma	306	3.9	2.9	144	3.6	162	4.2	0.86	234	3.9	44	4.5	0.87
Osteosarcoma	262	3.4	2.6	130	3.3	132	3.4	0.97	197	3.4	38	3.9	0.87
Ewing's sarcoma	208	2.8	2.1	109	2.8	99	2.6	1.08	194	3.3	3	0.3	11.00
All other histologic types	1713	21.8	16.4	860	21.4	853	22.6	0.95	1359	21.3	213	22.7	0.94

[a] Rates are standardized to the 1980 SEER population and reported per million children per year.

Source: From Bailey DL, Townsend DW, Valk PE, Maisey MN. Positron Emission Tomography: Basic Sciences. Springer-Verlag London Ltd 2005, p.759.

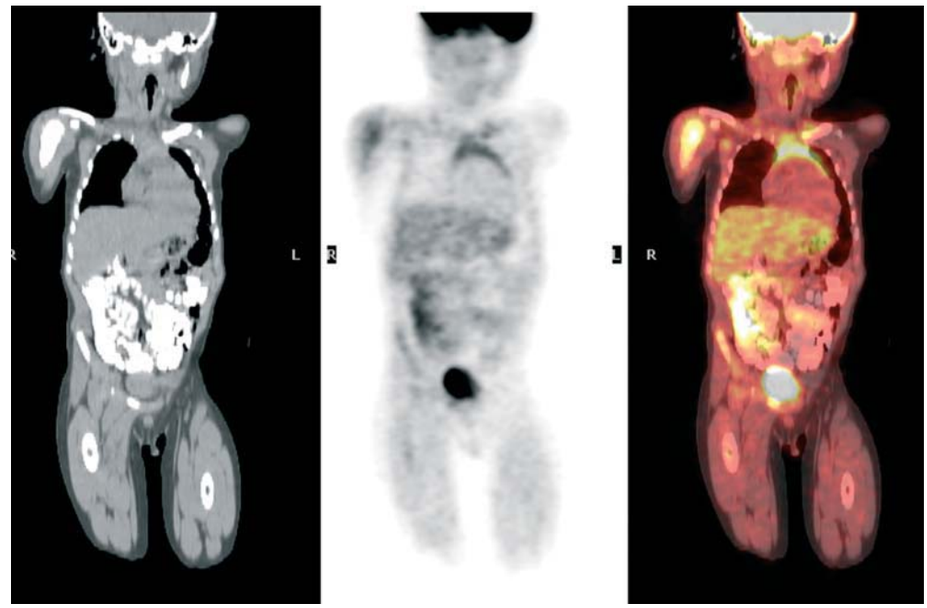

Figure 22.3. Five-year-old boy with history of T-cell large cell anaplastic lymphoma. Coronal images from PET/CT obtained before bone marrow transplantation. *Left panel:* CT of neck, chest, abdomen, pelvis, and thighs. *Center panel:* FDG-PET of same area shows normal-appearing thymic activity, left greater than right, in the superior mediastinum. *Right panel:* Fused PET/CT image overlays the metabolic information from the FDG-PET study onto the anatomic map provided by the CT images.

tration of hematopoietic stimulating factors may also resemble disseminated metastatic disease (Figure 22.5) (72, 73). Elevated bone marrow FDG uptake has been observed in patients as long as 4 weeks after completion of treatment with granulocyte colony-stimulating factor (G-CSF) (72). This observation is probably reflective of increased bone marrow glycolytic metabolism in response to hematopoietic growth factors.

Another important issue specific to PET imaging of pediatric patients is the choice of measurement parameter for the standardized uptake value (SUV), which is commonly used as a semiquantitative measure of the degree of FDG uptake in a region of interest. The calculation of SUV based on body surface area appears to be a more-uniform parameter than that calculated based on body weight in pediatric patients (74).

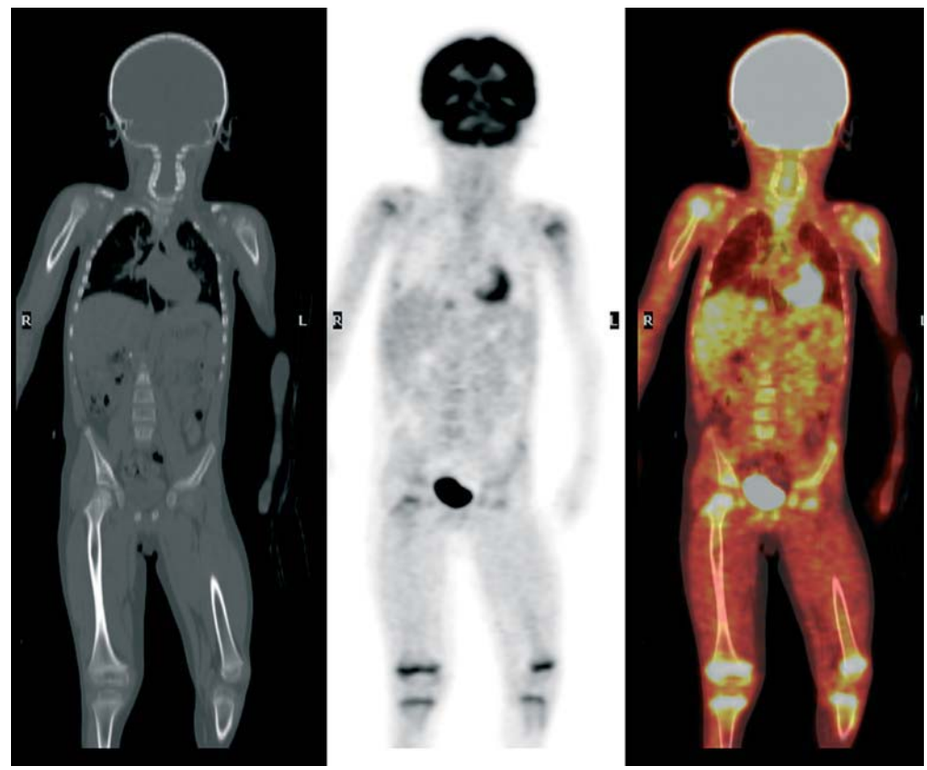

Figure 22.4. Coronal images of a 4-year-old boy with history of Wilms tumor. *Left panel:* CT images bone window. *Middle panel:* FDG-PET images show increased uptake representing growth plate activity in the proximal humerii, proximal femurs, and about both knees, similar to activity found in these areas on bone scan. *Right panel:* Fused FDG-PET images on CT show more precisely the anatomic location of the FDG activity representing growth plates.

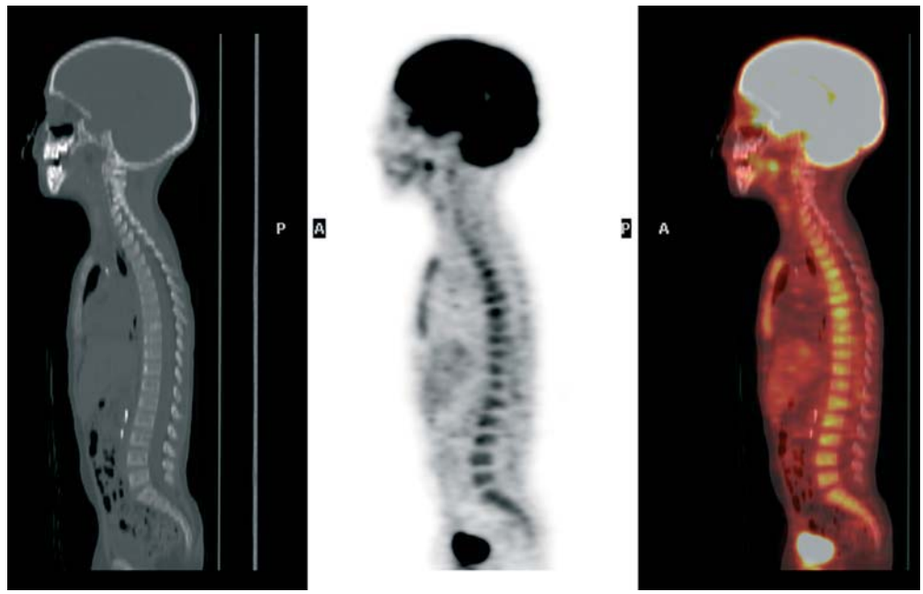

a b c

Figure 22.5. Sagittal images of PET/CT from 4-year-old child undergoing chemotherapy for metastatic Wilms tumor and receiving granulocyte colony-stimulating factor (G-CSF). (**a**) CT images bone window. (**b**) FDG-PET images show uniform increased uptake in the spine and sternum. (**c**) Fusion images of FDG-PET and CT.

Central Nervous System Tumors

Taken as a group, tumors of the central nervous system (CNS) are the most common nonhematologic tumors of childhood. They account for about 20% of all pediatric malignancies. The grouping includes many histologically diverse tumors of both neuroepithelial and nonneuroepithelial origin. The majority of pediatric brain tumors arise from neuroepithelial tissue. CNS tumors are subclassified histopathologically by cell type and graded for degree of malignancy using criteria that include mitotic activity, infiltration, and anaplasia (75, 76).

To grasp the wide variety of pediatric CNS tumors, one need only consider the distribution of the most common tumors according to the major anatomic compartment involved. In the posterior fossa, medulloblastoma, cerebellar astrocytoma, ependymoma, and brainstem gliomas are most common. Tumors about the third ventricle include tumors that arise from suprasellar, pineal, and ventricular tissue. The most common neoplasms about the third ventricle are optic and hypothalamic gliomas, craniopharyngiomas, and germ cell tumors. Supratentorial tumors are most often astrocytomas, many of which are low grade (76).

MRI and CT are the main imaging modalities used in staging and following children with CNS tumors. Their main limitation is the inability to distinguish viable recurrent or residual tumor from abnormalities resulting from surgery or radiation. SPECT with ^{201}Tl-chloride and ^{99m}Tc-methoxyisobutylisonitrile (MIBI) have proven valuable for this determination in a number of pediatric brain tumors (77–80). Use of FDG-PET in brain tumors has been widely reported in series that predominantly include adult patients for whom FDG-PET has helped distinguish viable tumor from posttherapeutic changes (81–83). High FDG uptake relative to adjacent brain indicates residual or recurrent tumor whereas low or absent FDG uptake is observed in areas of necrosis. This distinction is most readily made with high-grade tumors that show high uptake of FDG at diagnosis. Even with high-grade tumors, the presence of microscopic tumor foci is not excluded by an FDG-PET study that does not show increased uptake; this is particularly true after intensive radiation therapy, in which case FDG-PET results may not accurately correlate with tumor progression (84). Furthermore, in the immediate posttherapy period, elevated FDG uptake may persist (85).

FDG-PET has been applied to tumor grading and prognostic stratification. Higher-grade aggressive tumors typically have higher FDG uptake than do lower-grade tumors (Figures 22.6, 22.7) (86). Among low-grade tumors, some show insufficient FDG uptake to be distinguished from adjacent brain and some appear hypometabolic. The development of hypermetabolism as evidenced by increased

Figure 22.6. FDG-PET brain scan from a 10-year-old boy with anaplastic pontine astrocytoma shows considerably increased FDG uptake within the tumor compared to surrounding gray matter and extracerebral soft tissue. (**a**) coronal images; (**b**) sagittal images; (**c**) trans-

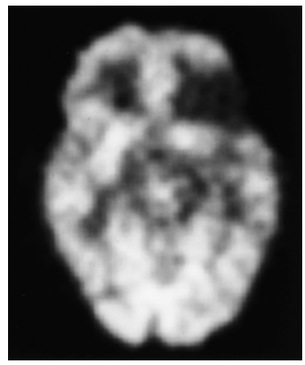

Figure 22.7. Transverse FDG-PET brain image from a 4.5-year-old boy with generalized tonic–clonic seizure demonstrates hypometabolism in the left frontal lobe. This area was resected and shown to be a low-grade glioma. (Reprinted with permission from Jadvar H, Connolly LP, Shulkin BL, Treves ST, Fischman AJ. Positron-emission tomography in pediatrics. Nuclear Medicine Annual 2000;53–83.)

FDG uptake in a low-grade tumor that appeared hypometabolic at diagnosis indicates degeneration to a higher grade (87). The biologic behavior of high-grade tumors may be reflected in their appearance on FDG-PET. Shorter survival times have been reported for patients whose tumors show the highest degree of FDG uptake (88). Data, although limited, suggest that FDG-PET findings also correlate well with pathology and clinical outcome in children (89–91). A potential pediatric application of this approach entails a reported excellent correlation between FDG-PET findings and clinical outcome in children affected by neurofibromatosis who have low-grade astrocytomas (92). In that series, high tumoral glucose metabolism shown by FDG-PET was a more-accurate predictor of tumor behavior than was histologic analysis. Combining FDG-PET imaging and MRI in the planning of stereotactic brain biopsies has been reported to improve the diagnostic yield in infiltrative, poorly defined lesions and to reduce sampling in high-risk functional areas (93).

Another positron-emitting radiotracer that has been used to study pediatric brain tumors is ^{11}C-methionine (^{11}C-Met), which localizes to only a minimal degree in normal brain. Uptake of this labeled amino acid reflects transmethylation pathways that are present in some tumors. However, as with FDG, some low-grade gliomas may escape detection (94, 95). ^{11}C-Met-PET has been reported to be useful in differentiating viable tumor from treatment-induced changes (94, 96). It is worth noting, however, that ^{11}C-Met is not tumor specific as it has been shown to accumulate in some nontumoral CNS diseases, probably as a result of blood–brain barrier disruption (97). Both FDG-PET and ^{11}C-Met-PET have been shown to be independent predictors of event-free survival (98). ^{11}C-Met, because of the short 20-min half-life of the ^{11}C label, must be produced locally for administration and is not commercially available.

Lymphoma

Lymphomas of non-Hodgkin's and Hodgkin's types cies. Non-Hodgkin's lymphoma occurs throughout childhood. Lymphoblastic and small cell tumors, including Burkitt's lymphoma, are the most common histologic types. The disease is usually widespread at diagnosis. Mediastinal and hilar involvement are common with lymphoblastic lymphoma. Burkitt's lymphoma most often occurs in the abdomen. Hodgkin's disease has a peak incidence during adolescence. Nodular sclerosing and mixed cellularity are the most common histologic types. The disease is rarely widespread at diagnosis and the majority of cases have intrathoracic nodal involvement (60, 99).

^{67}Ga-citrate scintigraphy has proven useful in staging and monitoring therapeutic response of patients with non-Hodgkin's and Hodgkin's lymphomas (100–104). In numerous studies, which have included predominantly adult patient populations, FDG has been shown to accumulate in non-Hodgkin's and Hodgkin's lymphoma tissue (Figure 22.8) (71, 105–123). Similarly to ^{67}Ga-citrate, FDG uptake is generally greater in higher- than in lower-grade lymphomas (112, 114). FDG-PET has been shown to reveal sites of nodal and extranodal disease that are not detected by conventional staging methods, resulting in upstaging of disease (110–117, 124). FDG-PET, when performed at the time of initial evaluation, has also been recently shown to change disease stage and treatment in up to 10% to 23% of children with lymphoma (125, 126). Identification of areas of intense FDG uptake within the bone marrow can be particularly useful in directing the site of biopsy or even eliminating the need for biopsy at staging (110, 123). FDG-PET is also useful for assessing residual soft tissue masses shown by CT after therapy. Absence of FDG uptake in a residual mass is predictive of remission whereas high uptake indicates residual or recurrent tumor (117). A negative FDG-PET scan after completion of chemotherapy, however, does not exclude the presence of residual microscopic disease (127). The potential role of FDG-PET in radiation treatment planning for pediatric oncology including lymphoma has also been recently described (128–130).

FDG-PET has been compared to ^{11}C-Met-PET in a relatively small series of 14 patients with non-Hodgkin's lymphoma. ^{11}C-Met-PET provided superior tumor-to-background contrast, whereas FDG-PET was superior in distinguishing between high- and low-grade lymphomas (108).

Neuroblastoma

Neuroblastoma is the most common extracranial solid malignant tumor in children. The mean age of patients at presentation is 20 to 30 months, and it is rare after the age of 5 years (99).

The most common location of neuroblastoma is the adrenal gland. Other sites of origin include the paravertebral and presacral sympathetic chain, the organ of Zuckerkandl, posterior mediastinal sympathetic ganglia, and cervical sympathetic plexuses. Gross or microscopic

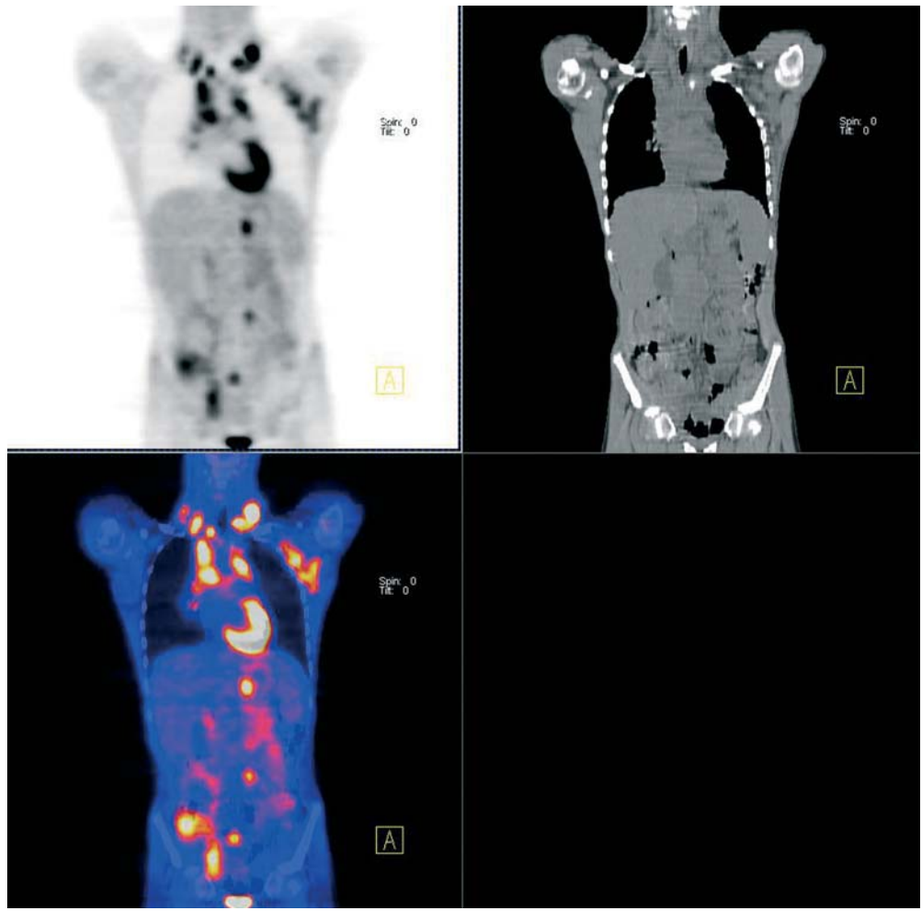

Figure 22.8. Coronal images of FDG-PET/CT of 11-year-old child with newly diagnosed nodular sclerosing Hodgkins disease following left axillary lymph node biopsy. *Upper left panel:* FDG-PET scan shows increased uptake of FDG in bilaterally in the lower neck and mediastinum, the left axilla, the right hilum, the left mid- and lower abdomen, and centrally within the pelvis. *Upper right panel:* CT image corresponding with FDG-PET scan. *Lower left panel:* Fusion image of these FDG-PET and CT images.

neural crest tumors, ganglioneuroma and ganglioneuroblastoma, have been described. Some neuroblastomas spontaneously regress or mature into ganglioneuroma, which is benign. However, the unpredictability and apparent infrequency of spontaneous regression and maturation, and the consequences of delaying therapy, require that treatment be instituted at diagnosis in most cases. Ganglioneuroblastoma is a malignant tumor that contains both undifferentiated neuroblasts and mature ganglion cells.

Disseminated disease is present in up to 70% of neuroblastoma cases at diagnosis and most commonly involves cortical bone and bone marrow. Less frequently, there is involvement of liver, skin, or lung. A primary tumor is not detected in up to 10% of children with disseminated neuroblastoma (131). The primary tumor may also go undetected in patients who present with paraneoplastic syndromes such as infantile myoclonic encephalopathy.

Surgical excision is the preferred treatment of localized neuroblastoma. When local disease is extensive, intensive preoperative chemotherapy may be utilized. When distant metastases are present, surgical removal is not likely to improve survival. The prognosis in these cases is poor, but high-dose chemotherapy, total-body irradiation, and bone marrow reinfusion are beneficial for some children

Delineation of local disease extent is achieved with MRI, CT, and scintigraphic studies (132). These tests are also utilized in localizing the primary site in children who present with disseminated disease or with a paraneoplastic syndrome. Metaiodobenzylguanidine (MIBG) and ^{111}In-pentetreotide scintigraphy have been employed in these settings with a sensitivity of greater than 85% for detecting neuroblastoma. Uptake of MIBG, which is an analogue of guanethidine and norepinephrine, into neuroblastoma is by a neuronal sodium- and energy-dependent transport mechanism. The localization of ^{111}In-pentetreotide in neuroblastoma reflects the presence of somatostatin type 2 receptors on some neuroblastoma cells (133).

Bone scintigraphy has been most widely used for detection of skeletal involvement for staging. MIBG and, to a lesser extent, ^{111}In-pentetreotide imaging have also been increasingly used for detecting skeletal involvement (134).

Patients with residual unresected primary tumors are periodically evaluated with MRI or CT. However, these studies cannot distinguish viable tumor from treatment-related scar or tumor that has matured into ganglioneuroma. Specificity in establishing residual viable tumor can be improved with MIBG or ^{111}In-pentetreotide

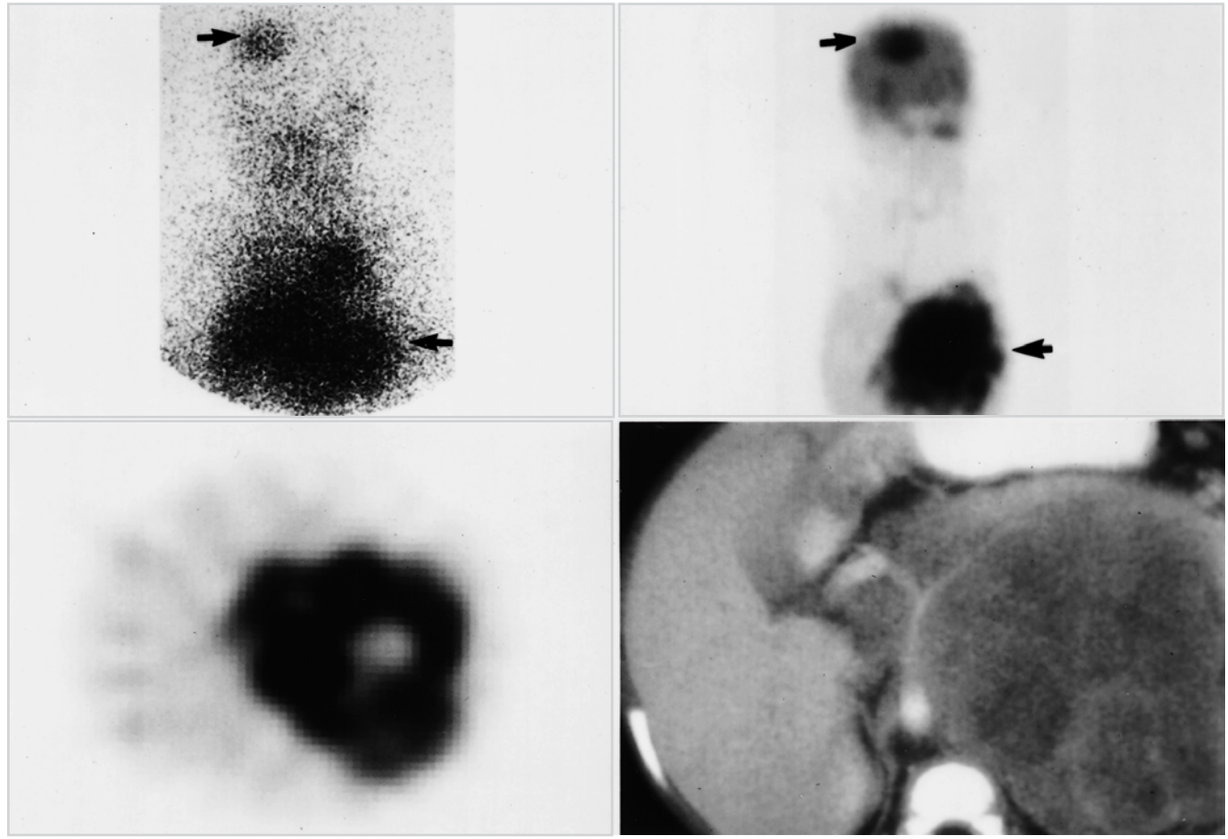

Figure 22.9. Images of a 2-year-old girl with neuroblastoma at presentation. *Top left:* Anterior planar view of the head, neck, chest, and upper abdomen 48 h following [^{131}I]MIBG injection. An area of abnormal uptake is present in the right superior aspect of the skull (*upper arrow*). A large focus of abnormal uptake in the primary tumor (*lower arrow*) extends from the upper left abdomen medially and inferior to the liver. *Top right:* Anterior projection of the head, neck, chest, and upper abdomen approximately 1 h following FDG injection. Increased FDG uptake in the skull (*upper arrow*) corresponding to the site of abnormal [^{131}I]MIBG uptake is well visualized against the normal brain uptake of FDG. Increased FDG uptake is present in the primary tumor (*lower arrow*). Note the paucity of background activity in the chest and abdomen. *Bottom left:* Transaxial image through the midabdomen shows marked FDG uptake in the primary tumor. A central area of decreased FDG accumulation probably represents necrosis. *Bottom right:* A large mass in the left abdomen is shown in a transaxial CT image. This set of images demonstrates that neuroblastomas are metabolically active. The primary tumor and metastases can be well visualized with FDG-PET. (Reprinted with permission from Jadvar H, Connolly LP, Shulkin BL, Treves ST, Fischman AJ. Positron-emission tomography in pediatrics. Nuclear Medicine Annual 2000;53–83.)

cumulate one of these agents. These agents are also useful in assessing residual skeletal disease in patients with MIBG- or ^{111}In-pentetreotide-avid skeletal metastases. Bone scintigraphy, however, is unable to distinguish active disease from bony repair on the basis of tracer uptake.

Neuroblastomas are metabolically active tumors. Neuroblastomas or their metastases avidly concentrated FDG before chemotherapy or radiation therapy in 16 of 17 patients studied with FDG-PET and MIBG imaging (135).Uptake after therapy was variable but tended to be lower. FDG and MIBG results were concordant in most instances (Figures 22.9, 22.10). However, there were occasions that one agent accumulated at a site of disease and the other did not (Figure 22.11). MIBG imaging was overall considered superior to FDG-PET, particularly in delineation of residual disease. As the patients in this series had aggressive tumors and poor prognoses, the value of FDG-PET for assessing therapeutic response could not be determined. An advantage of FDG-PET is the tion whereas MIBG imaging is performed 1 or more days following tracer administration.

FDG-PET imaging may be of limited value for the evaluation of the bone marrow involvement of neuroblastoma for reason of the mild FDG accumulation by the normal bone marrow (135). Pitfalls resulting from physiologic FDG uptake in the bowel and the thymus are additional factors that may limit the role for FDG-PET in neuroblastoma. A recent study has reported that once the primary tumor is resected, PET and bone marrow examination suffice for monitoring neuroblastoma patients at high risk for progressive disease in soft tissue, bone, and bone marrow (136). Currently, however, the primary role of FDG-PET in neuroblastoma is in the evaluation of known or suspected neuroblastomas that do not demonstrate MIBG uptake. We have also noted variable uptake of FDG in ganglioneuromas (Figure 22.12). This finding suggests that FDG may not reliably differentiate between neuroblastomas and ganglioneuromas.

^{11}C-Hydroxyephedrine (^{11}C-HED), an analogue of nor-

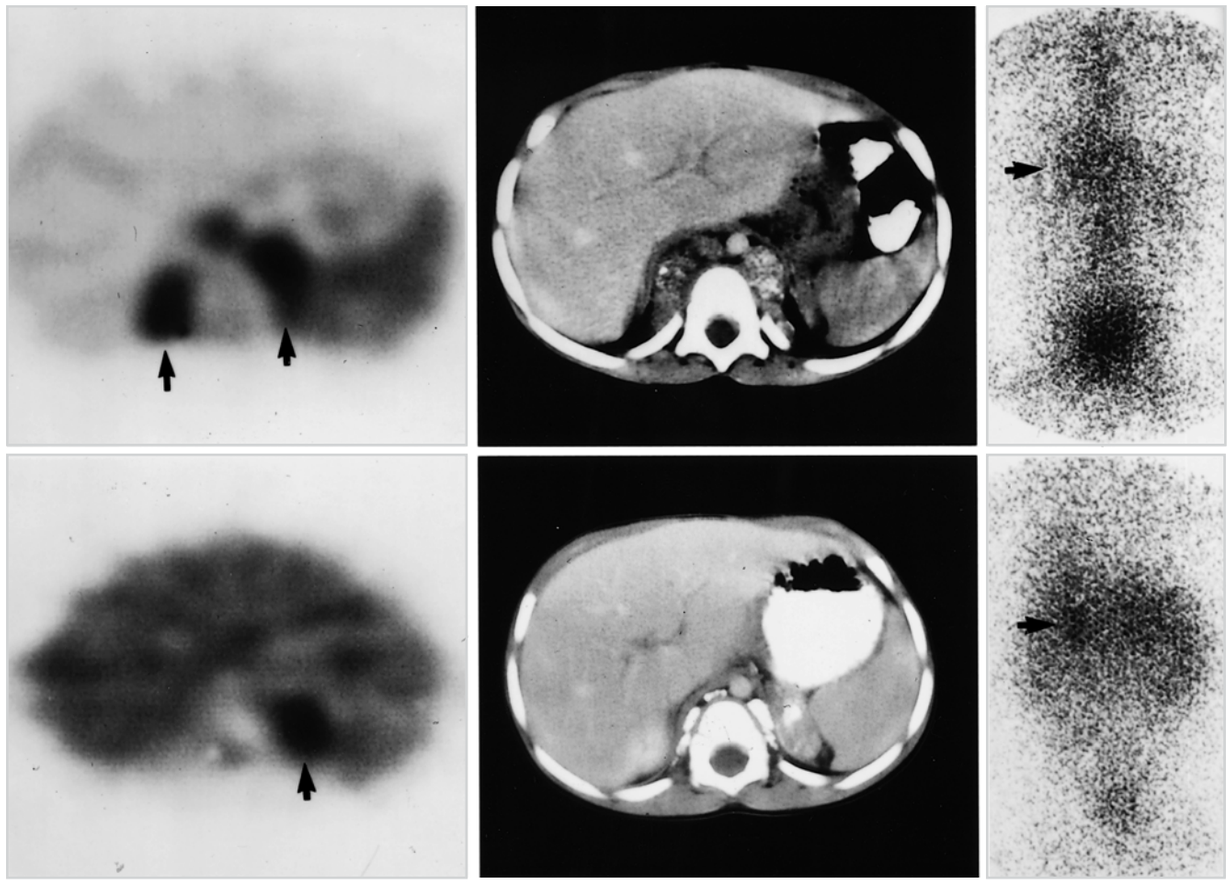

Figure 22.10. Three-year-old boy who presented with leg and abdominal pain: *top panel*, images from the time of diagnosis; *bottom panel*, images obtained at reevaluation 6 months later following chemotherapy. Following reevaluation, the patient underwent surgical exploration, and a tumor consisting of ganglioneuroblastoma was removed from the sites identified by MIBG scintigraphy and PET-FDG scanning the adrenal bed, and ganglioneuroma from the adjacent paraspinal lymphadenopathy, which no longer concentrated FDG. *Top left panel:* Transverse PET image of the upper abdomen acquired 60 min after injection. There is extensive paraspinal uptake of FDG (*arrows*). *Top middle panel:* CT scan demonstrates scattered calcifications within the paraspinal lymphadenopathy, which corresponds well with the increased metabolic activity demonstrated by FDG-PET scanning. *Top right panel:* Posterior image of the chest–abdomen–pelvis 48 h after [^{131}I]MIBG injection. There is a large area of abnormal uptake in the upper abdomen–lower thorax (*arrow*) and extensive uptake of MIBG within the skeleton, consistent with metastatic disease in the bone marrow. *Lower left panel:* Transverse PET image of the upper abdomen acquired at 60 min after injection shows persistent activity to the left of the spine, consistent with residual neoplasm (*arrow*). Uptake in paraspinal lymphadenopathy is no longer present. *Lower middle panel:* CT scan shows considerable calcification and reduction in the size of the paraspinal tumor, but a partially calcified mass persists in the region of the left adrenal gland. *Lower right panel:* Posterior image of the chest–abdomen 48 h after [^{131}I]MIBG injection. Slightly increased activity remains in the area of the left adrenal gland (*arrow*). (Reprinted with permission from Shulkin BL, Hutchinson RJ, Castle VP, Yanik GA, Shapiro B, Sisson JC. Neuroblastoma: positron emission tomography with 2-[fluorine-18]-fluoro-2-deoxy-D-glucose compared with metaiodobenzylguanidine scintigraphy. Radiology 1996;199:743–750.)

used in evaluating neuroblastoma (Figure 22.13). All seven neuroblastomas studied showed uptake of ^{11}C-HED (137), and four of five neuroblastomas studied showed uptake of ^{11}C-epinephrine (138). Uptake of these tracers is demonstrated within minutes after administration, which is an advantage over MIBG imaging. Limitations regarding cost and the need for onsite synthesis of short lived ^{11}C (half-life, 20 min) suggest that neither ^{11}C-HED nor ^{11}C-epinephrine PET is likely to replace MIBG imaging. These tracers may prove useful adjuncts in difficult cases where a primary tumor is difficult to identify with more readily available agents and to further the understanding of this disease. Compounds labeled with ^{18}F, such as fluoronorepinephrine, fluorometaraminol, and fluorodopamine, may also be useful tracers. PET (139) and ^{124}I-labeled MIBG (140) has also been described.

Wilms Tumor

Wilms tumor is the most common renal malignancy of childhood. Wilms tumor is predominantly seen in younger children and is uncommonly encountered after the age of 5 years (60). Bilateral renal involvement occurs in about 5% of all cases and can be identified synchronously or metachronously (97, 114). An asymptomatic abdominal mass is the typical mode of presentation. Nephrectomy with adjuvant chemotherapy is the treatment of choice. Radiation therapy is used in selected cases when resection is incomplete.

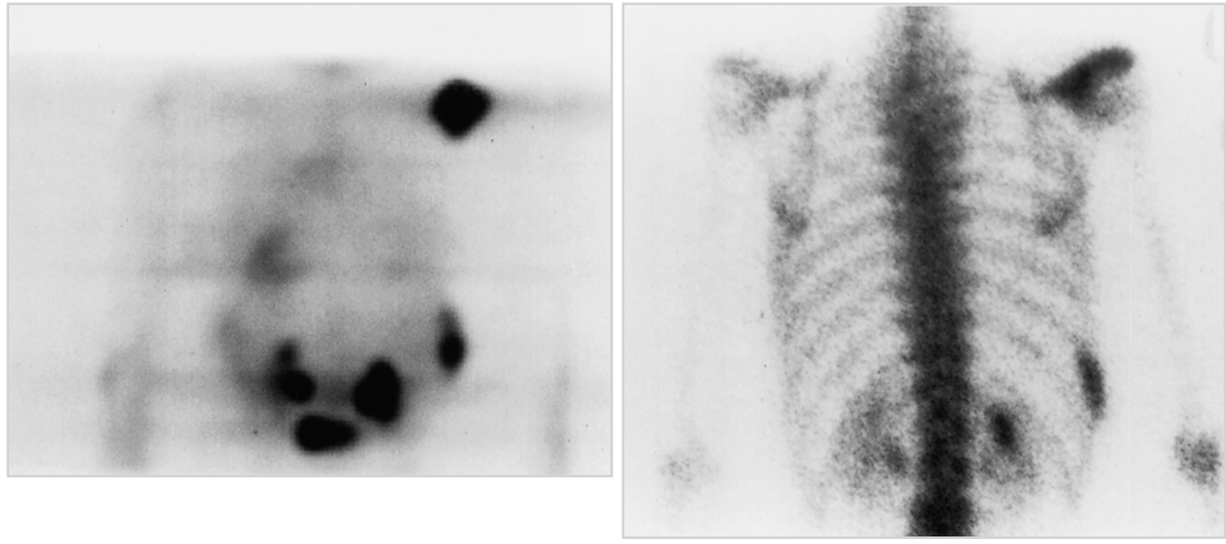

Figure 22.11. Neuroblastoma recurrence post bone marrow transplantation. *Left panel:* Posterior projection image of PET scan obtained 1 h following FDG injection. There is marked accumulation of FDG in the right shoulder (*arrow*), a right lower rib (*arrow*), and an abnormal focus of activity within the abdomen (*arrow*) between the kidneys, which most likely represented metastatic disease. *Right panel:* Posterior image of the chest and abdomen from a bone scan acquired 2 h following injection of 25 mCi [^{99m}Tc]MDP shows abnormal uptake in the right shoulder (*arrow*) and ninth right rib (*arrow*), confirming that two of the sites of abnormal FDG uptake involve bone. The patient declined further evaluation and died of widely metastatic disease. (Reprinted with permission from Shulkin BL, Hutchinson RJ, Castle VP, Yanik GA, Shapiro B, Sisson JC. Neuroblastoma: positron emission tomography with 2-[fluorine-18]-fluoro-2-deoxy-D-glucose compared with metaiodobenzylguanidine scintigraphy. Radiology 1996;199:743–750.)

Scintigraphy has not played an important role in imaging of Wilms tumor. Radiography, ultrasonography, CT, and MRI are commonly employed in anatomic staging and detection of metastases, which predominantly involve lung, occasionally liver, and only rarely other sites. Anatomic imaging, however, is of limited value in the assessment for residual or recurrent tumor (141). Uptake of FDG by Wilms tumor (Figure 22.14) has been described (142), but a role for FDG-PET in Wilms tumor has not been established. Normal excretion of FDG through the kidney is a limiting factor. However, careful correlation with anatomic cross-sectional imaging allows distinction of tumor uptake from normal renal FDG excretion.

Bone Tumors

Osteosarcoma and Ewing's sarcoma are the two primary bone malignancies of childhood; of the two, osteosarcoma is the more common and predominantly affects adolescents and young adults. A second peak affects older adults,

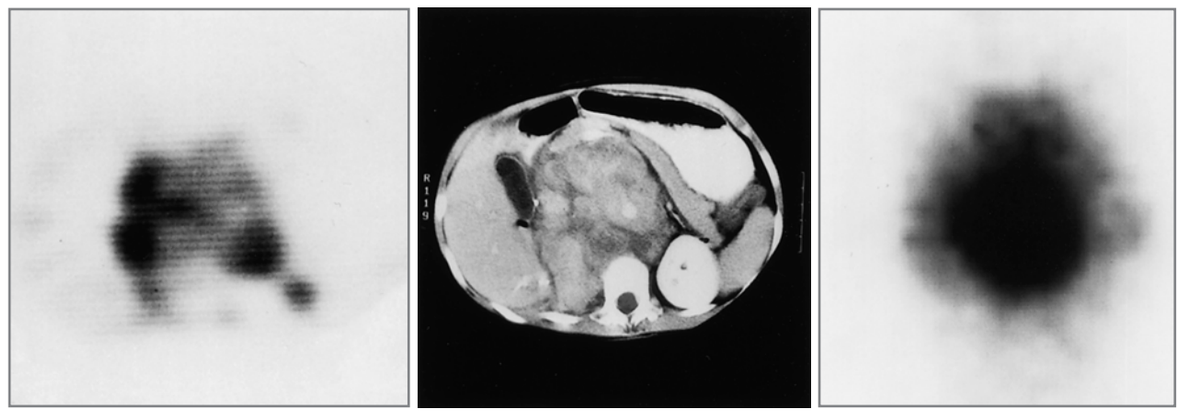

Figure 22.12. Uptake of FDG within ganglioneuroma. The patient presented at age 2 years with intractable diarrhea and was found to have a nonresectable 10-cm abdominal mass containing mostly stroma and rare elements of neuroblastoma. She received radiotherapy, chemotherapy, and subsequent surgical debulking. MIBG scans showed persistent abdominal uptake. The patient eventually received therapy with [^{131}I]MIBG. Surgical debulking was again repeated. Multiple resected portions of the tumor contained only mature stroma and no neuroblastoma. She did well and returned for reevaluation 16 months later. *Left panel:* Transverse image of PET scan obtained 60 min following injection of FDG shows heterogeneous increased uptake of FDG in midabdomen. *Middle panel:* CT scan of the abdomen demonstrates the very large abdominal mass. *Right panel:* Anterior image of [^{131}I]MIBG scan 48 h after injection shows extensive, intense uptake in the abdomen, corresponding to the tumor. (Reprinted with permission from Shulkin BL, Hutchinson RJ, Castle VP, Yanik GA, Shapiro B, Sisson JC. Neuroblastoma: positron emission tomography with 2-[fluorine-18]-fluoro-2-deoxy-D-glucose compared with metaiodobenzylguanidine scintigraphy. Radiology 1996;199:743–750.)

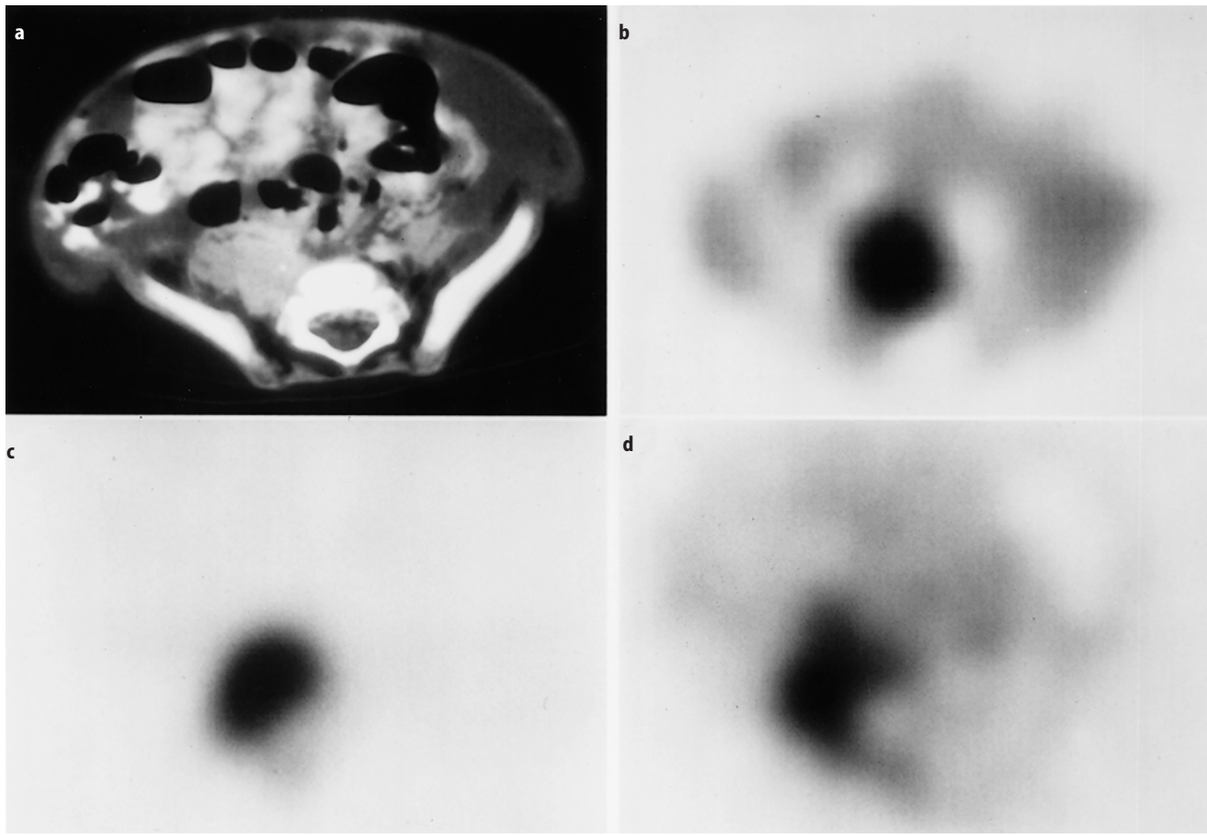

Figure 22.13. (**a**) CT scan of the pelvis of a 6-month-old boy following surgical debulking of abdominal–pelvic neuroblastoma. There is abnormal soft tissue with speckled calcification in the right posterior pelvis. (**b**) MIBG-SPECT scan at 24 h shows uptake into the tumor. (**c**) ^{11}C-Hydroxyephedrine (HED)-PET scan at 20 min following injection. There is excellent uptake within the neuroblastoma, and the image appears similar to the MIBG-SPECT examination. (**d**) FDG-PET scan at 50 min shows moderate accumulation of FDG within the mass relative to surrounding background. However, the tumor appears better delineated with the more specific adrenergic tumor imaging agent HED. (Reprinted by permission of the Society of Nuclear Medicine from Shulkin BL, Wieland DM, Baro ME, et al. PET hydroxyephedrine imaging of neuroblastoma. J Nucl Med 1996;37:18, Figure 2.)

predominantly individuals with a history of prior radiation to bone or Paget's disease. This tumor rarely affects children younger than 7 years of age. Osteosarcoma is typically a lesion of the long bones. The treatment of choice for osteosarcoma of an extremity is wide resection and limb-sparing surgery. Limb-sparing procedures entail the resection of tumor with a cuff of surrounding normal tissue at all margins, skeletal reconstruction, and muscle and soft tissue transfers. Employing current chemotherapeutic regimens pre- and postoperatively and imaging to define tumor extent and tumor viability preoperatively, limb-sparing procedures can be appropriately performed in 80% of patients with osteosarcoma (143).

Almost all cases of Ewing's sarcoma occur between the ages of 5 and 30 years with the highest incidence being in the second decade of life. In patients younger than 20 years, Ewing's sarcoma most often affects the appendicular skeleton. Beyond that age, pelvic, rib, and vertebral lesions predominate. The tumor is believed to be of neuroectodermal origin and, along with the primitive neuroectodermal tumor (PNET), to be part of a spectrum of a single biologic entity (144). Ewing's sarcoma is considered an undifferentiated variant and PNET a more differentiated peripheral neural tumor. Therapy for Ewing's sarcoma involves multiagent chemotherapy for eradication of microscopic or overt metastatic disease and irradiation and/or surgery for control of the primary lesion. Because late recurrence is not uncommon, resection of the primary tumor is gaining favor for local disease control (145).

MRI is used to define the local extent of osteosarcoma and Ewing's sarcoma in bone and soft tissue. However, signal abnormalities caused by peritumoral edema can result in an overestimation of tumor extension (146). Scintigraphy has been used primarily to detect skeletal metastases of these tumors at diagnosis and during follow-up. With osteosarcoma, skeletal scintigraphy occasionally demonstrates extraosseous metastases, most often pulmonary, as a result of osteoid production by the metastatic deposits.

Determination of preoperative chemotherapeutic response is important in planning limb salvage surgery. Because of the nonspecific appearance of viable tumor on MRI, variable results have been reported for assessing chemotherapeutic response (147–152). Scintigraphy with ^{201}Tl has been shown to be useful for assessing therapeutic response in osteosarcoma (153–158) and perhaps Ewing's sarcoma (154, 155). Marked decrease in tumoral ^{201}Tl uptake indicates a favorable response to

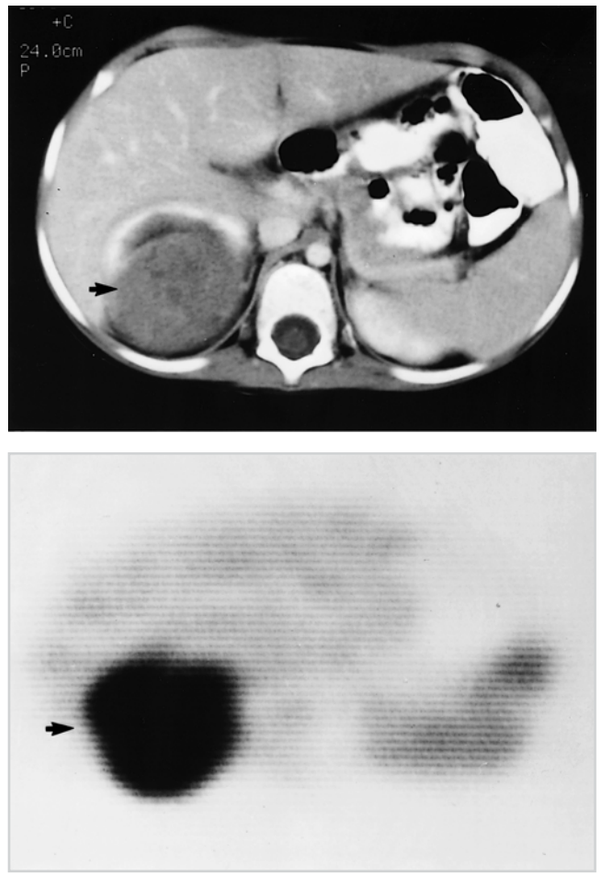

Figure 22.14. CT scan (**a**) PET scan (**b**). Markedly increased uptake of FDG (*arrow*) is present within the right-sided mass seen on CT (*arrow*). The mass was surgically removed and confirmed histologically to represent Wilms tumor. (Copyright 1997. From Shulkin BL, Chang E, Strouse PJ, et al. PET FDG studies of Wilms tumors. J Pediatr Hem/Onc 1997;19:334–338. Reproduced by permission of Taylor & Francis, Inc., http://www.taylorandfrancis.com.)

chemotherapy. When tumoral ^{201}Tl uptake does not decrease within weeks of chemotherapy, a therapeutic change may be needed. ^{99m}Tc-MIBI may also be useful in osteosarcoma but seemingly not with Ewing's sarcoma (159, 160).

The exact role of FDG-PET in osteosarcoma and Ewing's sarcoma has not yet been determined (Figures 22.15, 22.16). However, early experience suggests that in patients with Ewing's sarcoma FDG-PET may play a role in monitoring response to therapy (161–167). When compared to bone scintigraphy, FDG-PET may be superior for detecting osseous metastases from Ewing's sarcoma but may be less sensitive for those from osteosarcoma (168). A second potential role is in assessing patients with suspected or known pulmonary metastasis, which is particularly common with osteosarcoma.

Soft Tissue Tumors

Rhabdomyosarcoma is the most common soft tissue malignancy of childhood. The peak incidence occurs between 3 and 6 years of age. Rhabdomyosarcomas can develop in any organ or tissue but, contrary to what the name implies, this tumor does not usually arise in muscle. The most common anatomic locations are the head, particularly the orbit and paranasal sinuses, the neck, and the genitourinary tract. CT or MRI is important for establishing the extent of local disease. Radiography and CT are used for detecting pulmonary metastases, and skeletal scintigraphy is employed for identifying osseous metastases. Radiation therapy and surgery are utilized for local disease control, and chemotherapy is employed for treatment of metastases. Rhabdomyosarcomas show variable degrees of FDG accumulation. Cases showing the clinical utility of FDG-PET have been described, but the exact role of FDG-PET in rhabdomyosarcoma is yet to be determined (Figure 22.17) (4, 161).

Conclusion

FDG-PET is being applied increasingly to study diseases of childhood, especially tumors. Because the tumors encountered are relatively rare, it will be difficult to perform well-designed, prospective clinical trials at single institutions. The recent merger of the CCG (Children's Cancer Group) and the POG (Pediatric Oncology Group) to form COG (Children's Oncology Group) brings an opportunity to examine the use of FDG-PET in the management of childhood tumors in multiinstitutional, cooperative efforts. We expect that future data will show that FDG-PET does contribute unique, valuable information for the care of childhood tumors.

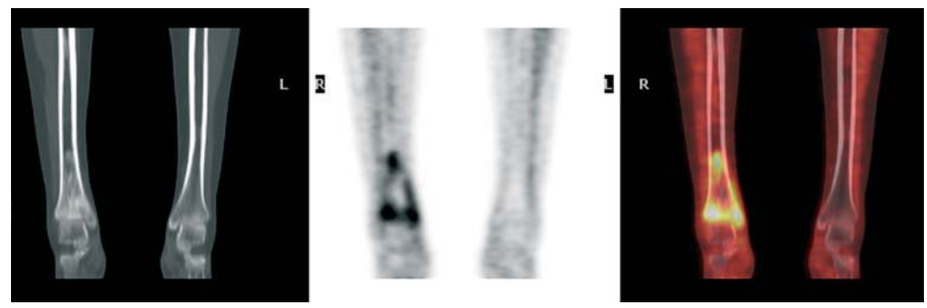

Figure 22.15. A 16-year-old girl with osteosarcoma. Images obtained following four courses of chemotherapy to assess for residual disease. (**a**) Coronal CT images show sclerotic lesions in the distal right tibia. (**b**) FDG-PET images show elevated FDG uptake at the periphery of the sclerotic lesions, indicating viable tumor. (**c**) Fusion images of CT and FDG-PET.

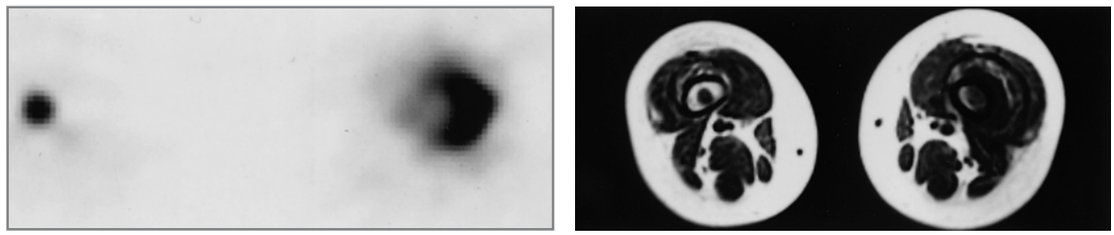

b (transverse)

a

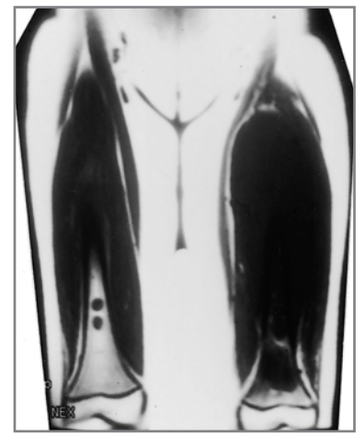

b (coronal)

Figure 22.16. An 11-year-old girl who complained of pain and swelling in the left thigh. Plain film radiographs showed findings suggestive of Ewing's sarcoma, subsequently confirmed on biopsy. (**a**) *Left panel:* Bone scan obtained 2 h following injection of ^{99m}Tc-MDP. Abnormal accumulation of tracer is noted throughout the left femur. The right femur is unremarkable. *Center panel:* Anterior projection image from PET study shows intense, irregular uptake of FDG within the soft tissues of the left thigh. Two small foci of activity are seen in the region of the distal right femur that are not present on bone scanning. *Right panel:* T_1-weighted coronal MR image shows soft tissue mass in the left thigh, replacement of normal marrow of the left femur, and two focal lesions in the distal right femur. (**b**) *Left panel:* Transverse and coronal image from PET scan at the level of the distal femurs. Intense uptake of FDG is present in the soft tissues surrounding the left femur and focally within the right femur. *Right panel:* T_1-weighted MR image at same level shows the soft tissue mass surrounding the left femur, replacement of marrow of the left femur, and a lesion in the center of the right femur. (Reprinted with permission from Shulkin BL, Mitchell DS, Ungar DR, et al. Neoplasms in a pediatric population: 2-[F-18]-fluoro-2-deoxy-D-glucose PET studies. Radiology 1995;194:495–500.)

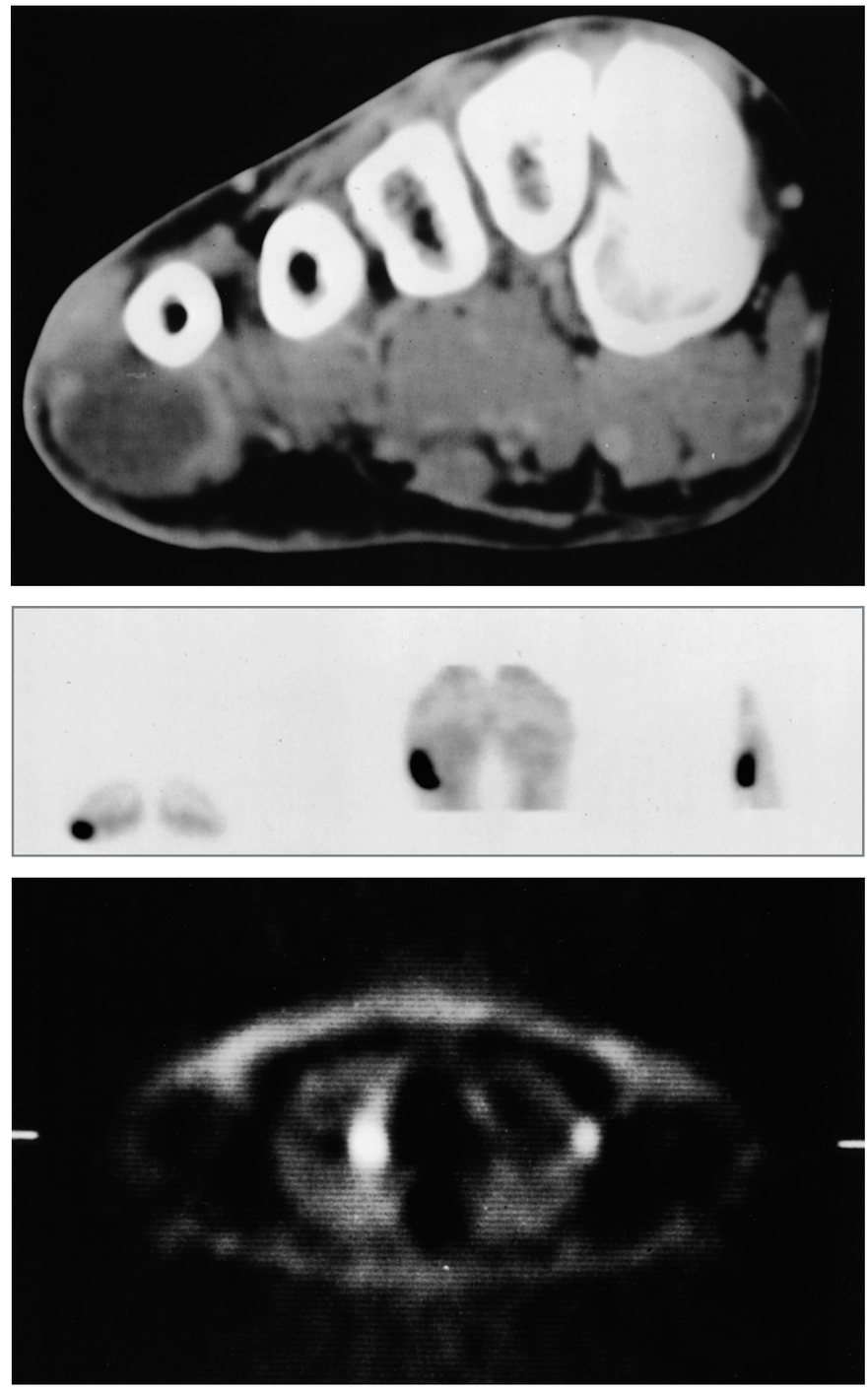

Figure 22.17. Rhabdomyosarcoma. (**a**) CT of the right foot of an 18-year-old girl following chemotherapy shows abnormal residual soft tissue mass below the right fifth metatarsal. (**b**) Depicted *left* to *right* are transverse, coronal, and sagittal images. (**c**) Nonattenuation-corrected images of the chest show metastases in the medial right lung and lateral left lung. (Reprinted with permission from Shulkin BL. PET applications in pediatrics. Q J Nucl Med 1997;41:281–291.)

Acknowledgments

Supported in part by grant NCI 54216 (BS). The authors thank Alan Fischman, M.D., Ph.D., for assistance with illustrations.

References

1. Gordon I. Issue surrounding preparation, information, and handling the child and parent in nuclear medicine. J Nucl Med 1998;39:490–494.

2. Treves ST. Introduction. In: Treves ST, editor. Pediatric Nuclear Medicine, 2nd ed. New York: Springer-Verlag, 1995:1–11.
3. Mandell GA, Cooper JA, Majd M, et al. Procedure guidelines for pediatric sedation in nuclear medicine. J Nucl Med 1997;38:1640–1643.
4. Shulkin BL. PET applications in pediatrics. Q J Nucl Med 1997;41:281–291.
5. Borgwardt L, Larsen HJ, Pedersen K, et al. Practical use and implementation of PET in children in a hospital PET center. Eur J Nucl Med Mol Imaging 2003;30:1389–1397.
6. Roberts EG, Shulkin BL. Technical issues in performing PET studies in pediatric patients. J Nucl Med Technol 2004;32:5–9.
7. Kaste SC. Issues specific to implementing PET/CT for pediatric oncology: what we have learned along the way. Pediatr Radiol 2004;34:205–213.
8. ICRP Report 80. Radiation dose to patients from radiopharmaceuticals. Stockholm: International Commission on Radiation Protection, 1998:49–110.
9. ICRP Report 56. Age-dependent doses to members of the public from intake of radionuclides: Part 1. Stockholm: International Commission on Radiation Protection, 1989:4.
10. Jones SC, Alavi A, Christman D, et al. The radiation dosimetry of 2-[^{18}F]fluoro-2-deoxy-D-glucose in man. J Nucl Med 1982;23:613–617.
11. Ruotsalainen U, Suhonen-Povli H, Eronen E, et al. Estimated radiation dose to the newborn in FDG-PET studies. J Nucl Med 1996;37:387–393.
12. Fahey F, Palmer M, Strauss K, et al. Image quality and dosimetry using CT-based attenaution correction. (In preparation.)
13. Brenner D, Elliston C, Hall E, et al. Estimated risks of radiation-induced fatal cancer from pediatric CT. Am J Radiol 2001;176:289–296.
14. Chugani HT, Phelps ME. Maturational changes in cerebral function in infants determined by ^{18}FDG positron emission tomography. Science 1986;231:840–843.
15. Chugani HT, Phelps ME, Mazziotta JC. Positron emission tomography study of human brain functional development. Ann Neurol 1987;22:487–497.
16. Chugani HT. Positron emission tomography. In: Berg BO, editor. Principles of Child Neurology. New York: McGraw-Hill, 1996:113–128.
17. Hauser W. Epidemiology of epilepsy in children. Neurosurg Clin N Am 1995;6:419–428.
18. National Institutes of Health Consensus Development Conference Statement: surgery for epilepsy. Epilepsia ;31:806–812.
19. Kuzniecky R, Suggs S, Gaudier J, et al. Lateralization of epileptic foci by magnetic resonance imaging in temporal lobe epilepsy. J Neuroimaging 1991;1:163–167.
20. Treves ST, Connolly LP. Single photon emission computed tomography in pediatric epilepsy. Neurosurg Clin N Am 1995;6:473–480.
21. Snead OC III, Chen LS, Mitchell WG, et al. Usefulness of [^{18}F]fluorodeoxyglucose positron emission tomography in pediatric epilepsy surgery. Pediatr Neurol 1996;14:98–107.
22. Meltzer CC, Adelson PD, Brenner RP, et al. Planned ictal FDG PET imaging for localization of extratemporal epileptic foci. Epilepsia 2000;41(2):193–200.
23. Juhasz C, Chugani DC, Muzik O, et al. Is epileptogenic cortex truly hypometabolic on interictal positron emission tomography? Ann Neurol 2000;48(1):88–96.
24. Cummings TJ, Chugani DC, Chugani HT. Positron emission tomography in pediatric epilepsy. Neurosurg Clin N Am 1995;6:465–472.
25. Engel J Jr, Kuhl DE, Phelps ME. Patterns of human local cerebral glucose metabolism during epileptogenic seizures. Science 1982;218:64–66.
26. da Silva EA, Chugani DC, Muzik O, et al. Identification of frontal lobe epileptic foci in children using positron emission tomography. Epilepsia 1997;38:1198–1208.
27. Hrachovy R, Frost J. Infantile spasms. Pediatr Clin N Am 1989;36:311–329.
28. Chugani HT, Shields WD, Shewmon DA, et al. Infantile spasms: I. PET identifies focal cortical dysgenesis in cryptogenic cases for surgical treatment. Ann Neurol 1990;27:406–413.
29. Chuagni HT, Shewmon DA, Shields WD, et al. Surgery for intractable infantile spasms: neuroimaging perspectives. Epilepsia 1993;34:764–771.
30. Chugani HT, Da Silva E, Chugani DC. Infantile spasms: III. Prognostic implications of bitemporal hypometabolism on positron emission tomography. Ann Neurol 1996;39:643–649.
31. Chugani HT, Conti JR. Etiologic classification of infantile spasms in 140 cases: role of positron emission tomography. J Child Neurol 1996;11:44–48.
32. Savic I, Svanborg E, Thorell JO. Cortical benzodiazepine receptor changes are related to frequency of partial seizures: a positron emission tomography study. Epilepsia 1996;37:236–244.
33. Arnold S, Berthele A, Drzezga A, et al. Reduction of benzodiazepine receptor binding is related to the seizure onset zone in extratemporal focal cortical dysplasia. Epilepsia 2000;41(7):818–824.
34. Richardson MP, Koepp MJ, Brooks DJ, et al. ^{11}C-Flumanezil PET in neocortical epilepsy. Neurology 1998;51:485–492.
35. Debets RM, Sadzot B, van Isselt JW, et al. Is ^{11}C-flumazenil PET superior to ^{18}FDG PET and ^{123}I-iomazenial SPECT in presurgical evaluation of temporal lobe epilepsy? J Neurol Neurosurg Psychiatry 1997;62:141–150.
36. Kumlien E, Hartvig P, Valind S, et al. NMDA-receptor activity visualized with (*S*)-[*N*-methyl-11-C]ketamine and positron emission tomography in patients with medial temporal epilepsy. Epilepsia 1999;40:30–37.
37. Mayberg HS, Sadzot B, Meltzer CC, et al. Quantification of mu and non-mu opiate receptors in temporal lobe epilepsy using positron emission tomography. Ann Neurol 1991;30:3–11.
38. Kumlien E, Bergstrom M, Lilja A, et al. Positron emission tomography with [C-11]deuterium deprenyl in temporal lobe epilepsy. Epilepsia 1995;36:712–721.
39. Volpe JJ, Herscovitch P, Perlman JM, et al. Positron emission tomography in the newborn: extensive impairment of regional cerebral blood flow with intraventricular hemorrhage and hemorrhagic intracerebral involvement. Pediatrics 1983; 72(5):589–601.
40. Volpe JJ, Herscovitch P, Perlman JM, et al. Positron emission tomography in the asphyxiated term newborn: parasagittal impairment of cerebral blood flow. Ann Neurol 1985;17(3):287–296.
41. Zilbovicius M, Boddaert N, Belin P, et al. Temporal lobe dysfunction in childhood autism: a PET study. Am J Psychiatry 2000;157(12):1988–1993.
42. Ernst M, Zametkin AJ, Matochik JA, et al. High midbrain [^{18}F]DOPA accumulation in children with attention deficit hyperactivity disorder. Am J Psychiatry 1999;156(8):1209–1215.
43. Jacobson LK, Hamburger SD, Van Horn JD, et al. Cerebral glucose metabolism in childhood onset schizophrenia. Psychiatry Res 1997;75(3):131–144.
44. Reed W, Jagust W, Al-Mateen M, et al. Role of positron emission tomography in determining the extent of CNS ischemia in patients with sickle cell disease. Am J Hematol 1999;60(4):268–272.
45. Delvenne V, Lotstra F, Goldman S, et al. Brain hypometabolism of glucose in anorexia nervosa: a PET scan study. Biol Psychiatry 1995;37(3):161–169.
46. Delvenne V, Goldman S, Simon Y, et al. Brain hypometabolism of glucose in bulimia nervosa. Int J Eat Disord 1997;21(4):313–320.
47. Lee JS, Asano E, Muzik O, et al. Sturge-Weber syndrome: correlation between clinical course and FDG PET findings. Neurology 2001;57:189–195.
48. Al-Essa MA, Bakheet SM, Patay ZJ, et al. Clinical and cerebral FDG PET scan in a patient with Krabbe's disease. Pediatr Neurol 2000;22:44–47.
49. Lee JS, Juhasz C, Kaddurah AK, et al. Patterns of cerebral glucose metabolism in early and late stages Rasmussen's syndrome. J Child Neurol 2001;16:798–805.

50. Lee JS, PfundZ, Juhasz C, et al. Altered regional brain glucose metabolism in Duchenne muscular dystrophy: a PET study. Muscle Nerve 2002;26:506–512.
51. Quinlivan RM, Robinson RO, Maisey MN. Positron emission tomography in pediatric cardiology. Arch Dis Child 1998;79(6):520–522.
52. Donnelly JP, Raffel DM, Shulkin BL, et al. Resting coronary flow and coronary flow reserve in human infants after repair or palliation of congenital heart defects as measured by positron emission tomography. J Thorac Cardiovasc Surg 1998;115(1):103–110.
53. Yates RW, Marsden PK, Badawi RD, et al. Evaluation of myocardial perfusion using positron emission tomography in infants following a neonatal arterial switch operation. Pediatr Cardiol 2000;21(2):111–118.
54. Rickers C, Sasse K, Buchert R, et al. Myocardial viability assessed by positron emission tomography in infants and children after the arterial switch operation and suspected infarction. J Am Coll Cardiol 2000;36(5):1676–1683.
55. Singh TP, Muzik O, Forbes TF, et al. Positron emission tomography myocardial perfusion imaging in children with suspected coronary abnormalities. Pediatr Cardiol 2003;24:138–144.
56. Hernandez-Pampaloni M, Allada V, Fishbein MC, et al. Myocardial perfusion and viability by positron emission tomography in infants and children with coronary abnormalities: correlation with echocardiography, coronary angiography, and histopathology. J Am Coll Cardiol 2003;41:618–626.
57. Hwang B, Liu RS, Chu LS, et al. Positron emission tomography for the assessment of myocardial viability in Kawasaki disease using different therapies. Nucl Med Commun 2000;21(7):631–636.
58. Huaser M, Bengel F, Kuehn A, et al. Myocardial blood flow and coronary flow reserve in children with "normal" epicardial coronary arteries after the onset of Kawasaki disease assessed by positron emission tomography. Pediatr Cardiol 2004; 25:108–112.
59. Litvinova I, Litvinov M, Loeonteva I, et al. PET for diagnosis of mitochondrial cardiomyopathy in children. Clin Posit Imaging 2000;3(4):172.
60. Gurney JG, Severson RK, Davis S, et al. Incidence of cancer in children in the United States. Cancer (Phila) 1995;75:2186–2195.
61. Robison L. General principles of the epidemiology of childhood cancer. In: Pizzo P, Poplack D, editors. Principles and Practice of Pediatric Oncology. Philadelphia: Lippincott-Raven, 1997:1–10.
62. Franzius C, Schober O. Assessment of therapy response by FDG PET in pediatric patients. Q J Nucl Med 2003;47:41–45.
63. Wegner EA, Barrington SF, Kingston JE, et al. Eur J Nucl Med Mol Imaging 2005;32(1):23–30.
64. Shulkin BL. PET imaging in pediatric oncology. Pediatr Radiol 2004;34:199–204.
65. Patel PM, Alibazoglu H, Ali A, et al. Normal thymic uptake of FDG on PET imaging. Clin Nucl Med 1996;21:772–775.
66. Weinblatt ME, Zanzi I, Belakhlef A, et al. False positive FDG-PET imaging of the thymus of a child with Hodgkin's disease. J Nucl Med 1997;38:888–890.
67. Brink I, Reinhardt MJ, Hoegerle S, et al. Increased metabolic activity in the thymus gland studied with 18F-FDG PET: age dependency and frequency after chemotherapy. J Nucl Med 2001;42:591–595.
68. Yeung HW, Grewal RK, Gonen M, et al. Patterns of (18F)-FDG uptake in adipose tissue and muscles: a potential source of false-positives for PET. J Nucl Med 2003;44:1789–1796.
69. Cohade C, Mourtzikos KA, Wahl RL. "USA-fat": prevalence is related to ambient outdoor temperature: evaluation with ^{18}F-FDG PET/CT. J Nucl Med 2003;44:1267–1270.
70. Tatsumi M, Engles JM, Ishimori T, et al. Intense (18)F-FDG uptake in brown fat can be reduced pharmacologically. J Nucl Med 2004;45:1189–1193.
71. Delbeke D. Oncological applications of FDG PET imaging: colorectal cancer, lymphoma, and melanoma. J Nucl Med 1999;40:591–603.
72. Sugawara Y, Fisher SJ, Zasadny KR, et al. Preclinical and clinical studies of bone marrow uptake of fluorine-1-fluorodeoxyglucose with or without granulocyte colony-stimulating factor during chemotherapy. J Clin Oncol 1998;16:173–180.
73. Hollinger EF, Alibazoglu H, Ali A, et al. Hematopoietic cytokine-mediated FDG uptake simulates the appearance of diffuse metastatic disease on whole-body PET imaging. Clin Nucl Med 1998;23:93–98.
74. Yeung HW, Sanches A, Squire OD, et al. Standardized uptake value in pediatric patients: an investigation to determine the optimum measurement parameter. Eur J Nucl Med Mol Imaging 2002;29:61–66.
75. Kleihues P, Burger P, Scheithauer B. The new WHO classification of brain tumours. Brain Pathol 1993;3:255–268.
76. Robertson R, Ball WJ, Barnes P. Skull and brain. In: Kirks D, editor. Practical Pediatric Imaging. Diagnostic Radiology of Infants and Children. Philadelphia: Lippincott-Raven, 1997:65–200.
77. Maria B, Drane WB, Quisling RJ, et al. Correlation between gadolinium-diethylenetriaminepentaacetic acid contrast enhancement and thallium-201 chloride uptake in pediatric brainstem glioma. J Child Neurol 1997;12:341–348.
78. O'Tuama L, Janicek M, Barnes P, et al. Tl-201/Tc-99m HMPAO SPECT imaging of treated childhood brain tumors. Pediatr Neurol 1991;7:249–257.
79. O'Tuama L, Treves ST, Larar G, et al. Tl-201 versus Tc-99m MIBI SPECT in evaluation of childhood brain tumors. J Nucl Med 1993;34:1045–1051.
80. Rollins N, Lowry P, Shapiro K. Comparison of gadolinium-enhanced MR and thallium-201 single photon emission computed tomography in pediatric brain tumors. Pediatr Neurosurg 1995;22:8–14.
81. Valk PE, Budinger TF, Levin VA, et al. PET of malignant cerebral tumors after interstitial brachytherapy. Demonstration of metabolic activity and correlation with clinical outcome. J Neurosurg 1988;69:830–838.
82. Di Chiro G, Oldfield E, Wright DC, et al. Cerebral necrosis after radiotherapy and/or intraarterial chemotherapy for brain tumors: PET and neuropathologic studies. Am J Radiol 1988;150:189–197.
83. Glantz MJ, Hoffman JM, Coleman RE, et al. Identification of early recurrence of primary central nervous system tumors by [^{18}F]fluorodeoxyglucose positron emission tomography. Ann Neurol 1991;29:347–355.
84. Janus T, Kim E, Tilbury R, et al. Use of [^{18}F]fluorodeoxyglucose positron emission tomography in patients with primary malignant brain tumors. Ann Neurol 1993;33:540–548.
85. Rozental JM, Levine RL, Nickles RJ. Changes in glucose uptake by malignant gliomas: preliminary study of prognostic significance. J Neurooncol 1991;10:75–83.
86. Schifter T, Hoffman JM, Hanson MW, et al. Serial FDG-PET studies in the prediction of survival in patients with primary brain tumors. J Comput Assist Tomogr 1993;17:509–561.
87. Francavilla TL, Miletich RS, Di Chiro G, et al. Positron emission tomography in the detection of malignant degeneration of low-grade gliomas. Neurosurgery 1989;24:1–5.
88. Patronas NJ, Di Chiro G, Kufta C, et al. Prediction of survival in glioma patients by means of positron emission tomography. J Neurosurg 1985;62:816–822.
89. Molloy PT, Belasco J, Ngo K, et al. The role of FDG PET imaging in the clinical management of pediatric brain tumors. J Nucl Med 1999;40:129P (abstract).
90. Holthof VA, Herholz K, Berthold F, et al. In vivo metabolism of childhood posterior fossa tumors and primitive neuroectodermal tumors before and after treatment. Cancer (Phila) 1993;1394–1403.
91. Hoffman JM, Hanson MW, Friedman HS, et al. FDG-PET in pediatric posterior fossa brain tumors. J Comput Assist Tomogr 1992;16:62–68.
92. Molloy PT, Defeo R, Hunter J, et al. Excellent correlation of FDG PET imaging with clinical outcome in patients with neurofibromatosis type I and low-grade astrocytomas (abstract). J Nucl Med 1999;40:129P.

93. Pirotte B, Goldman S, Salzberg S, et al. Combined positron emission tomography and magnetic resonance imaging for the planning of stereotactic brain biopsies in children: experience in 9 cases. Pediatr Neurosurg 2003;38:146–155.
94. O'Tuama LA, Phillips PC, Strauss LC, et al. Two-phase [^{11}C]L-methionine PET in childhood brain tumors. Pediatr Neurol 1990;6:163–170.
95. Mosskin M, von Holst H, Bergstrom M, et al. Positron emission tomography with ^{11}C-methionine and computed tomography of intracranial tumours compared with histopathologic examination of multiple biopsies. Acta Radiol 1987;28:673–681.
96. Lilja A, Lundqvist H, Olsson Y, et al. Positron emission tomography and computed tomography in differential diagnosis between recurrent or residual glioma and treatment-induced brain lesion. Acta Radiol 1989;38:121–128.
97. Mineura K, Sasajima T, Kowada M, et al. Indications for differential diagnosis of nontumor central nervous system diseases from tumors. A positron emission tomography study. J Neuroimaging 1997;7:8–15.
98. Utriainen M, Metsahonkala L, Salmi TT, et al. Metabolic characterization of childhood brain tumors: comparison of ^{18}F-fluorodeoxyglucose and ^{11}C-methionine positron emission tomography. Cancer (Phila) 2002;95:1376–1386.
99. Cohen MD. Imaging of Children with Cancer. St. Louis: Mosby Yearbook, 1992.
100. Nadel HR, Rossleigh MA. Tumor imaging. In: Treves ST, editor. Pediatric Nuclear Medicine, 2nd ed. New York: Springer-Verlag, 1995:496–527.
101. Rossleigh MA, Murray IPC, Mackey DWJ. Pediatric solid tumors: evaluation by gallium-67 SPECT studies. J Nucl Med 1990;31:161–172.
102. Howman-Giles R, Stevens M, Bergin M. Role of gallium-67 in management of paediatric solid tumors. Aust Paediatr J 1982;18:120–125.
103. Yang SL, Alderson PO, Kaizer HA, et al. Serial Ga-67 citrate imaging in children with neoplastic disease: concise communication. J Nucl Med 1979;20:210–214.
104. Sty JR, Kun LE, Starshak RJ. Pediatric applications in nuclear oncology. Semin Nucl Med 1985;15:17–200.
105. Barrington SF, Carr R. Staging of Burkitt's lymphoma and response to treatment monitored by PET scanning. Clin Oncol 1995;7:334–335.
106. Bangerter M, Moog F, Buchmann I, et al. Whole-body 2-[^{18}F]-fluoro-2-deoxy-D-glucose positron emission tomography (FDG PET) for accurate staging of Hodgkin's disease. Ann Oncol 1998;9:1117–1122.
107. Jerusalem G, Warland V, Najjar F, et al. Whole-body ^{18}F-FDG PET for the evaluation of patients with Hodgkin's disease and non-Hodgkin's lymphoma. Nucl Med Commun 1999;20:13–20.
108. Leskinen-Kallio S, Ruotsalainen U, Nagren K, et al. Uptake of carbon-11-methionine and fluorodeoxyglucose in non-Hodgkin's lymphoma:a PET study. J Nucl Med 1991;32:1211–1218.
109. Moog F, Bangerter M, Kotzerke J, et al. 18-F-Fluorodeoxyglucose positron emission tomography as a new approach to detect lymphomatous bone marrow. J Clin Oncol 1998;16:603–609.
110. Moog F, Bangerter M, Diederichs CG, et al. Extranodal malignant lymphoma: detection with FDG PET versus CT. Radiology 1998;206:475–481.
111. Moog F, Bangerter M, Diederichs CG, et al. Lymphoma: role of whole-body 2-deoxy-2-[F-18]fluoro-D-glucose (FDG) PET in nodal staging. Radiology 1997;203:795–800.
112. Okada J, Yoshikawa K, Imazeki K, et al. The use of FDG-PET in the detection and management of malignant lymphoma: correlation of uptake with prognosis. J Nucl Med 1991;32:686–691.
113. Okada J, Yoshikawa K, Itami M, et al. Positron emission tomography using fluorine-18-fluorodeoxyglucose in malignant lymphoma: a comparison with proliferative activity. J Nucl Med 1992;33:325–329.
114. Rodriguez M, Rehn S, Ahlstrom H, et al. Predicting malignancy grade with PET in non-Hodgkin's lymphoma. J Nucl Med 1995;36:1790–1796.
115. Paul R. Comparison of fluorine-18-2-fluorodeoxyglucose and gallium-67 citrate imaging for detection of lymphoma. J Nucl Med 1987;28:288–292.
116. Newman JS, Francis IR, Kaminski MS, et al. Imaging of lymphoma with PET with 2-[F-18]-fluoro-2-deoxy-D-glucose: correlation with CT. Radiology 1994;190:111–116.
117. de Wit M, Bumann D, Beyer W, et al. Whole-body positron emission tomography (PET) for diagnosis of residual mass in patients with lymphoma. Ann Oncol 1997;8(suppl 1):57–60.
118. Cremerius U, Fabry U, Neuerburg J, et al. Positron emission tomography with 18-F-FDG to detect residual disease after therapy for malignant lymphoma. Nucl Med Commun 1998;19:1055–1063.
119. Hoh CK, Glaspy J, Rosen P, et al. Whole-body FDG PET imaging for staging of Hodgkin's disease and lymphoma. J Nucl Med 1997;38:343–348.
120. Romer W, Hanauske AR, Ziegler S, et al. Positron emission tomography in non-Hodgkin's lymphoma: assessment of chemotherapy with fluorodeoxyglucose. Blood 1998;91:4464–4471.
121. Stumpe KD, Urbinelli M, Steinert HC, et al. Whole-body positron emission tomography using fluorodeoxyglucose for staging of lymphoma: effectiveness and comparison with computed tomography. Eur J Nucl Med 1998;25:721–728.
122. Lapela M, Leskinen S, Minn HR, et al. Increased glucose metabolism in untreated non-Hodgkin's lymphoma: a study with positron emission tomography and fluorine-18-fluorodeoxyglucose. Blood 1995;86:3522–3527.
123. Carr R, Barrington SF, Madan B, et al. Detection of lymphoma in bone marrow by whole-body positron emission tomography. Blood 1998;91:3340–3346.
124. Hudson MM, Krasin MJ, Kaste SC. PET imaging in pediatric Hodgkin's lymphoma. Pediatr Radiol 2004;34:190–198.
125. Montravers F, McNamara D, Landman-Parker J, et al. [(18)F]FDG in childhood lymphoma: clinical utility and impact on management. Eur J Nucl Med Mol Imaging 2002;29:1155–1165.
126. Depas G, De Barsy C, Jerusalem G, et al. ^{18}F-FDG PET in children with lymphomas. Eur J Nucl Med Mol Imaging 2005;32(1):31–38.
127. Lavely WC, Delbeke D, Greer JP, et al. FDG PET in the follow-up of management of patients with newly diagnosed Hodgkin and non-Hodgkin lymphoma after first-line chemotherapy. Int J Radiat Oncol Biol Phys 2003;57:307–315.
128. Swift P. Novel techniques in the delivery of radiation in pediatric oncology. Pediatr Clin N Am 2002;49:1107–1129.
129. Korholz D, Kluge R, Wickmann L, et al. Importance of F18-fluorodeoxy-D-2-glucose positron emission tomography (FDG-PET) for staging and therapy control of Hodgkin's lymphoma in childhood and adolescence: consequences for the GPOH-HD 2003 protocol. Onkologie 2003;26:489–493.
130. Krasin MJ, Hudson MM, Kaste SC. Positron emission tomography in pediatric radiation oncology: integration in the treatment-planning process. Pediatr Radiol 2004;34:214–221.
131. Bousvaros A, Kirks DR, Grossman H. Imaging of neuroblastoma: an overview. Pediatr Radiol 1986;16:89–106.
132. Kushner BH. Neuroblastoma: a disease requiring a multitude of imaging studies. J Nucl Med 2004;45:1172–1188.
133. Briganti V, Sestini R, Orlando C et al. Imaging of somatostatin receptors by indium-111-pentetreotide correlates with quantitative determination of somatostatin receptor type 2 gene expression in neuroblastoma tumor. Clin Cancer Res 1997;3:2385–3291.
134. Shulkin BL, Shapiro B, Hutchinson RJ. ^{131}I-MIBG and bone scintigraphy for the detection of neuroblastoma. Presented at the Fifth Biennial Congress of the South African Society of Nuclear Medicine, Capetown, South Africa, September, 1992. S Afr Med J 1993;83:53.
135. Shulkin BL, Hutchinson RJ, Castle VP, et al. Neuroblastoma: positron emission tomography with 2-[fluorine-18]-fluoro-2-deoxy-D-glucose compared with metaiodobenzylguanidine scintigraphy. Radiology 1996;199:743–750.
136. Kushner BH, Yeung HW, Larson SM, et al. Extending positron emission tomography scan utility to high-risk neuroblastoma:

fluorine-18 fluorodeoxyglucose positron emission tomography as sole imaging modality in follow-up of patients. J Clin Oncol 2001;19:3397–3405.
137. Shulkin BL, Wieland DM, Baro ME, et al. PET hydroxyephedrine imaging of neuroblastoma. J Nucl Med 1996;37:16–21.
138. Shulkin BL, Wieland DM, Castle VP, et al. Carbon-11 epinephrine PET imaging of neuroblastoma. J Nucl Med 1999;40:129P (abstract).
139. Vaidyanathan G, Affleck DJ, Zalutsky MR. Validation of 4-[fluorine-18]fluoro-3-iodobenzylguanidine as a positron-emitting analog of MIBG. J Nucl Med 1995;36:644–650.
140. Ott RJ, Tait D, Flower MA, et al. Treatment planning for ^{131}I-mIBG radiotherapy of neural crest tumors using ^{124}I-mIBG positron emission tomography. Br J Radiol 1992;65:787–791.
141. Barnewolt CE, Paltiel HJ, Lebowitz RL, et al. Genitourinary system. In: Kirks DR, editor. Practical Pediatric Imaging. Diagnostic Radiology of Infants and Children, 3rd edition. Philadelphia: Lippincott-Raven, 1997:1009–1170.
142. Shulkin BL, Chang E, Strouse PJ, et al. PET FDG studies of Wilms tumors. J Pediatr Hematol/Onccol 1997;19:334–338.
143. McDonald DJ. Limb salvage surgery for sarcomas of the extremities. Am J Radiol 1994;163:509–513.
144. Triche TJ. Pathology of pediatric malignancies. In: Pizzo PA, Poplack DG, editors. Principles and Practice of Pediatric Oncology, 2nd ed. Philadelphia: Lippincott, 1993:115–152.
145. O'Connor MI, Pritchard DJ. Ewing's sarcoma. Prognostic factors, disease control, and the reemerging role of surgical treatment. Clin Orthop 1991;262:78–87.
146. Jaramillo D, Laor T, Gebhardt M. Pediatric musculoskeletal neoplasms. Evaluation with MR imaging. MRI Clin N Am 1996;4:1–22.
147. Frouge C, Vanel D, Coffre C, et al. The role of magnetic resonance imaging in the evaluation of Ewing sarcoma: a report of 27 cases. Skeletal Radiol 1988;17:387–392.
148. MacVicar AD, Olliff JFC, Pringle J, et al. Ewing sarcoma: MR imaging of chemotherapy-induced changes with histologic correlation. Radiology 1992;184:859–864.
149. Lemmi MA, Fletcher BD, Marina NM, et al. Use of MR imaging to assess results of chemotherapy for Ewing sarcoma. Am J Radiol 1990;155:343–346.
150. Erlemann R, Sciuk J, Bosse A, et al. Response of osteosarcoma and Ewing sarcoma to preoperative chemotherapy: assessment with dynamic and static MR imaging and skeletal scintigraphy. Radiology 1990;175:791–796.
151. Holscher HC, Bloem JL, Vanel D, et al. Osteosarcoma: chemotherapy-induced changes at MR imaging. Radiology 1992;182:839–844.
152. Lawrence JA, Babyn PS, Chan HS, et al. Extremity osteosarcoma in childhood: prognostic value of radiologic imaging. Radiology 1993;189:43–47.
153. Connolly LP, Laor T, Jaramillo D, et al. Prediction of chemotherapeutic response of osteosarcoma with quantitative thallium-201 scintigraphy and magnetic resonance imaging. Radiology 1996;201(P):349 (abstract).
154. Lin J, Leung WT. Quantitative evaluation of thallium-201 uptake in predicting chemotherapeutic response of osteosarcoma. Eur J Nucl Med 1995;22:553–555.
155. Menendez LR, Fideler BM, Mirra J. Thallium-201 scanning for the evaluation of osteosarcoma and soft tissue sarcoma. J Bone Joint Surg 1993;75:526–531.
156. Ramanna L, Waxman A, Binney G, et al. Thallium-201 scintigraphy in bone sarcoma: comparison with gallium-67 and technetium-99m MDP in the evaluation of chemotherapeutic response. J Nucl Med 1990;31:567–572.
157. Rosen G, Loren GJ, Brien EW, et al. Serial thallium-201 scintigraphy in osteosarcoma. Correlation with tumor necrosis after preoperative chemotherapy. Clin Orthop 1993;293:302––306.
158. Ohtomo K, Terui S, Yokoyama R, et al. Thallium-201 scintigraphy to assess effect of chemotherapy to osteosarcoma. J Nucl Med 1996;37:1444–1448.
159. Bar-Sever Z, Connolly LP, Treves ST, et al. Technetium-99m MIBI in the evaluation of children with Ewing's sarcoma. J Nucl Med 1997;38:13P (abstract).
160. Caner B, Kitapel M, Unlu M, et al. Technetium-99m-MIBI uptake in benign and malignant bone lesions: a comparative study with technetium-99m-MDP. J Nucl Med 1992;33:319–324.
161. Lenzo NP, Shulkin B, Castle VP, et al. FDG PET in childhood soft tissue sarcoma. J Nucl Med 2000;41(suppl 5):96P (abstract).
162. Abdel-Dayem HM. The role of nuclear medicine in primary bone and soft tissue tumors. Semin Nucl Med 1997;27:355–363.
163. Shulkin BL, Mitchell DS, Ungar DR, et al. Neoplasms in a pediatric population: 2-[F-18]-fluoro-2-deoxy-D-glucose PET studies. Radiology 1995;194:495–500.
164. Jadvar H, Connolly LP, Shulkin BL, et al. Positron-emission tomography in pediatrics. Nucl Med Annual 2000;53–83.
165. Franzius C, Sciuk J, Brinkschmidt C, et al. Evaluation of chemotherapy response in primary bone tumors with F-18 FDG positron emission tomography compared with histologically assessed tumor necrosis. Clin Nucl Med 2000;25:874–881.
166. Hawkins DS, Rajendran JG, Conrad EU III, et al. Evaluation of chemotherapy response in pediatric bone sarcomas by [F-18]-fluorodeoxy-D-glucose positron emission tomography. Cancer (Phila) 2002;94:3277–3284.
167. Brisse H, Ollivier L, Edeline V, et al. Pediatr Radiol 2004;34:595–605.
168. Franzius C, Sciuk J, Daldrup-Link HE, et al. FDG-PET for detection of osseous metastases from malignant primary bone tumors: comparison with bone scintigraphy. Eur J Nucl Med 2000;27:1305–1311.